Quasiparticle properties of quantum Hall ferromagnets

Marcus Kasner,[1,2] J. J. Palacios,[1,3,4] and A. H. MacDonald[1]
[1]*Department of Physics, Indiana University, Swain Hall West 117, Bloomington, Indiana 47405*
[2]*Institut für Theoretische Physik, Otto-von-Guericke-Universität Magdeburg, PF 4120, D-39016 Magdeburg, Germany*
[3]*Department of Physics and Astronomy, University of Kentucky, Lexington, Kentucky 40506-0055*
[4]*Departamento de Fisica Teorica de la Materia Condensada, Universidad Autonoma de Madrid, Cantoblanco, Madrid 28049, Spain*
(Received 6 March 2000)

We report on a study of the temperature and Zeeman-coupling-strength dependence of the one-particle Green's function of a two-dimensional (2D) electron gas at a Landau-level filling factor $\nu=1$, where the ground state is a strong ferromagnet. Our work places emphasis on the role played by the itinerancy of the electrons which carry the spin magnetization, and on analogies between this system and conventional itinerant electron ferromagnets. We go beyond self-consistent-field theory by evaluating the one-particle Green's function using a self-energy, which accounts for quasiparticle spin-wave interactions. Our calculations predict a sharp peak at a large bias voltage in the 2D-2D tunneling current, with an integrated strength that increases approximately linearly with temperature. We compare calculated properties with experiment, where available, and with predictions based on numerical exact diagonalization and other theoretical approaches.

I. INTRODUCTION

The physics of a two-dimensional electron system (2DES) in a magnetic field is in many respects unique. Since the degeneracy of the discrete Landau levels increases in proportion to the magnetic-field strength, all electrons can be accommodated in the lowest Landau level (LLL) for sufficiently strong fields. A Landau level then behaves, in many respects, like a band of zero width, and the system can be regarded as the extreme limit of a strongly correlated narrow-band electronic system. In this paper we focus on spin magnetism of the electron system at a Landau-level filling factor $\nu=1$ corresponding, when the spin degree of freedom is accounted for, to the case of a half-filled ''Landau band.'' At this filling factor, it is known[1,2] that, when disorder can be neglected, the ground state of the 2DES is ferromagnetic. We are motivated to study this system because it encompasses many of the difficulties[3] which have confounded attempts to build a complete theory of metallic ferromagnetic systems, yet is free of the troubling but incidental consequences of a complex band structure. The finite-temperature properties of metallic ferromagnets are more involved than those of insulating ferromagnets, because of the importance of both spin and charge degrees of freedom, so much so that much early theory was based on misguided attempts to assign magnetic and conducting properties to separate classes of electrons. Despite an immense effort and many advances,[3] no completely satisfactory theory of metallic ferromagnets exists. Progress toward understanding metallic ferromagnets has been hampered in part by the quantitative importance of details of the electronic band structure, which may not be accurately known or which may be difficult to render faithfully in going beyond mean-field theories of many-body effects. The present system has no such difficulties. We regard the quantum Hall ferromagnet as a laboratory for testing theories of interplay between quasiparticle and collective magnetic degrees of freedom in metallic magnets. In this work we predict the appearance at finite temperatures of a large-bias peak in the tunneling conductance between these 2D ferromagnets due to long-wavelength collective fluctuations in the spin-magnetization organization.

Our work is also motivated in part by recent experimental progress. Barrett *et al.*[4] were able to measure the temperature dependence of the spin-polarization and nuclear-spin-relaxation rates at fixed filling factors around $\nu=1$ using nuclear magnetic resonance techniques. Later, Manfra *et al.*[5] extracted the spin magnetization from magneto-optical-absorption measurements. It is our hope that critical comparison between experiment and theory will yield insights with wider relevance to the finite temperature properties of itinerant electron ferromagnets. It is, however, important to recognize that the 2DES at $\nu=1$ is different from conventional itinerant electron ferromagnets in several important ways. Most importantly, two dimensionality implies that its spontaneous spin magnetic moment will not survive at finite temperatures ($T_c=0$.) In addition, the strong magnetic field, which through its coupling to the electron's orbital degrees of freedom produces Landau levels, also produces a Zeeman coupling to electron's spin degree of freedom. For the most studied 2DES's, those formed at $GaAs/Al_xGa_{1-x}As$ heterojunctions, the Zeeman coupling is quite small compared to both Landau-level separations and the characteristic interaction energy scale. As we discuss below, the main effect of Zeeman coupling at low temperatures is to cut off the decrease of the magnetization due to the thermal excitation of very long-wavelength spin waves, and to mitigate consequences of the system's reduced dimensionality.

The recent experimental work stimulated two different theoretical approaches, which focus on different aspects of the spin-magnetization physics. Read and Sachdev[6] compared experimental data with large-N limits of a quantum continuum field theory model, which provides an accurate description of the long-wavelength collective behavior of the electronic spins. In this theory, physical properties are dependent only on the two independent ratios between the thermal energy k_BT, the Zeeman coupling strength Δ_z, and the

spin-stiffness energy ρ_s. Recently this work was extended by Timm *et al.*[7] The field-theory description is expected[8] to be accurate at low temperature when the Zeeman coupling strength is weak. This approach achieves a reasonable overall agreement between theory and experiment, at least at low temperatures. Our work has a different motivation and follows a different line. We are interested in addressing the temperature dependence of the underlying electronic structure, as it changes in concert with the change in the spin magnetization. Hence we focus on the one-particle Green's function. A brief account of some parts of this work was published previously.[9] From the Green's function we can calculate the electronic spectral function and hence the magnetization, the tunneling density of states, and (if vertex corrections are neglected) the nuclear-spin-relaxation time. The approximation we use is one which accounts for the interaction of quasiparticles with thermally excited spin waves. This approximation has deficiencies. At low temperatures and at low Zeeman energies the magnetizations we calculate do not appear to be in quite as good agreement with experiment as magnetizations from large-N approximations in the field-theory calculations. At medium and high temperatures, we do not account systematically for temperature-dependent screening effects which are likely to be important. Some progress in the latter direction was recently reported by Haussmann,[10] whose bosonized self-consistent random-phase approximation yields satisfying results at high temperatures, but fails at low temperatures. Progress on these fronts, which can be checked by comparison with experiment, may suggest routes toward more generically satisfactory theories of itinerant electron ferromagnets.

Our paper is organized as follows. In Sec. II we briefly review established results for the ground state and elementary excitations of the 2DES at $\nu=1$, which will be important for subsequent discussion. The ground state has all spins aligned by an arbitrarily weak Zeeman coupling. If we neglect Landau-level mixing, and we do throughout this paper, this state has no pure charge excitations. Its elementary excitations all have a single reversed spin. It turns out that, in the quantum Hall regime, the Hartree-Fock approximation (HFA) is exact for the ground state, and the time-dependent Hartree-Fock approximation is exact for its elementary excitations. The situation is therefore similar to that for many typical metallic ferromagnets, where there is substantial evidence that the ground state is well described by the Hartree-Fock-like Kohn-Sham equations[11] of the spin-density-functional formalism, and that its elementary excitations are well described by a time-dependent generalization of density-functional theory. In Sec. III we discuss the application of the self-consistent Hartree-Fock approximation at finite temperature. The failure of this approximation at finite temperatures is analogous to the well-known failure of the band theory of magnetism to provide even a rough account of the ordering temperature. The approximation, on which the present work is based, is discussed in Sec. IV. We obtain an expression for the electronic self-energy by analytically evaluating a particle-hole ladder summation involving Green's functions of opposite spin. We emphasize that in our microscopic theory, it is essential to account for screening even in the low-temperature limit. Section V discusses results for the spin magnetization, the spin-lattice relaxation rate, and the temperature-dependent 2D-2D tunneling I-V relation, all based on this self-energy approximation. In this section we also compare our results with available experiments, with other approximate theories, and with data from finite-size numerical calculations of the magnetization and magnetic susceptibility. We conclude that it is necessary to account for the finite thickness of the quantum well in comparing with experiment, and that the magnetization will be overestimated at high temperatures by models which do not account for electronic itinerancy. We predict the occurrence of a sharp peak, with a strength approximately proportional to the temperature, in the tunneling I-V relation when eV is close to the zero-temperature spin-splitting. In Sec. VI we discuss some aspects of our calculation which point to difficulties in developing a completely satisfactory microscopic theory. Finally, we conclude in Sec. VII with a brief summary.

II. STRONG-FIELD LIMIT PRELIMINARIES

In this paper we deal with a two-dimensional electron system where the electrons are subject to a constant perpendicular magnetic field of strength $\vec{B}=B\vec{e}_z$. We are particularly interested in the situation at filling factor $\nu=1$, so that the number of electrons in the system (N) equals the number of single-particle orbitals available in each Landau level: $N_\phi=AB/\Phi_0$. A is the area of the two-dimensional system, and $\Phi_0=h/e$ is the magnetic-flux quantum. One of the underlying assumptions in our model is that the Landau level-separation is large enough that we can ignore fluctuations in which electrons occupy higher orbital Landau levels. This requires that the Zeeman gap and the interaction strength be sufficiently small in comparison to $\hbar\omega_c$ where $\omega_c=eB/m^*$ is the cyclotron frequency. The microscopic Hamiltonian in the Landau gauge $[\vec{A}=(0,Bx,0)]$ is then[12]

$$H=-\frac{1}{2}\Delta_z(N_\uparrow-N_\downarrow)+\frac{\lambda}{2}\sum_{\substack{p,p',q\\ \sigma,\sigma'}}\tilde{W}(q,p-p')\times c^\dagger_{p+(q/2),\sigma}c^\dagger_{p'-(q/2),\sigma'}c_{p'+(q/2),\sigma'}c_{p-(q/2),\sigma}, \quad (1)$$

where $\lambda=e^2/(4\pi\epsilon l_c)$ is the interaction coupling constant, $\Delta_z=|g\mu_B B|$ is the Zeeman energy, and $p=k_y=2\pi l/L_y$, ($l=0,\pm1,\ldots$) are the momenta in y direction. The magnetic length $l_c=\sqrt{\hbar/|eB|}$ is used as the unit of length below. When Landau-level mixing is neglected, the kinetic-energy term in the Hamiltonian is constant ($N\hbar\omega_c/2$), and is therefore neglected. In Eq. (1), $N_\sigma=\Sigma_p c^\dagger_{p,\sigma}c_{p,\sigma}$ is the number operator for an electron with spin σ. We choose $\sigma=\uparrow$ as the direction parallel to the external magnetic field.

In the Landau gauge the two-particle matrix element is given by[12]

$$\tilde{W}(q,p-p')=\frac{1}{L_y}\int_{-\infty}^{\infty}\frac{dk_x}{2\pi}\tilde{V}(k_x,q)e^{-[(k_x^2+q^2)/2]l_c^2}e^{ik_x(p-p')l_c^2}, \quad (2)$$

where $\tilde{V}(\vec{k})$ is the Fourier transform of the effective 2D Coulomb interaction, which may include modifications to account for the finite thickness of the quantum well containing

the electrons or, as we discuss below, the *ad hoc* incorporation of screening effects. The interaction vertex is a function only of q, the momentum transfer due to the interaction, and $p-p'$, the momentum difference of the interacting particles. In the physically realistic case of long-range Coulomb interactions between the electrons, it is necessary to incorporate a neutralizing positive background by setting $\tilde{V}(k_x,k_y) \propto \Sigma_p \tilde{W}(q=0,p)=0$. Note that the interaction term is similar to that of a one-dimensional interacting fermion model with spin-split bands of zero width. However, in the present case $\tilde{W}$ depends not only on the transferred momentum q, but also on the momentum difference of the incoming or outgoing particles. This would be true even if we choose a hard-core interaction in real space $V(\vec{r})=4\pi V_0 \delta^{(2)}(\vec{r}/l_c)$. For this model, the matrix element $\tilde{W}(q,p-p')$ becomes $V_0\sqrt{2/\pi}e^{-(q^2/2-(p-p')^2)l_c^2/2}$.

Unlike most interacting electron systems, screening of mutual interactions does not play a major role in the correlation physics of a quantum Hall ferromagnet, at least at low temperatures. In fact, static screening in this limit is weak because of the gap for charged excitations of the ground state. Nevertheless, below we obtain the somewhat surprising result that the electron self-energy has a weak divergence if screening is completely neglected. For this reason we allow for the *ad hoc* inclusion of screening effects in our calculations by substituting for the Fourier transform of the Coulomb interaction, $\tilde{V}_c(\vec{k})=2\pi l_c/k$, the local static screening form $\tilde{V}(\vec{k})=2\pi l_c/(k+k_{sc})$. The constant value assigned to the screening wave vector k_{sc} is discussed below.

The Green's functions we calculate at a particular temperature depend, up to an overall energy scale, only on the ratio Δ_z/λ. At typical field strengths this ratio is small, even though λ varies approximately as $B^{1/2}$ while Δ_z is proportional to B. For example,[4] at a magnetic field of $B=7T$, $\Delta_z/\lambda \simeq 2.2K/136K=0.016$. Thus we will be interested primarily in the case where the interaction term dominates over the one-particle spin-dependent term.

We now briefly recount some known results for the ground state and low-lying excitations of the strong-field Hamiltonian. We start by considering the case of vanishing Zeeman coupling. If the interaction is of the hard-core type, the ground state at filling factor $\nu=1$ can be determined[1] by identifying zero-energy eigenstates of the positive definite Hamiltonian. It turns out that these must be the product of the the Slater determinant ($|\Psi_S\rangle$) constructed from all N_ϕ one-particle orbitals in the lowest Landau level and a many-particle spinor. The antisymmetry property of the many-fermion wave function then requires that the spinor be completely symmetric. From this it follows that it has total spin quantum number $S=N/2$. By this argument we are able to establish with some rigor that the ground state at $\nu=1$ is a strong ferromagnet, in agreement[13] with the Hartree-Fock approximation discussed in Sec. III, and if we regard the degenerate Landau level as analogous to an open atomic shell, with Hund's rule arguments. An infinitesimal Zeeman coupling selects from this spin multiplet a ground state, in which all spins are aligned; for a Zeeman field in the $\hat{z}$ direction the ground state has $S^z=S=N/2$, and the nondegenerate ground-state wave function is given exactly by the only state in the $\nu=1$ many-fermion Hilbert space, which has these quantum numbers:

$$|\Psi_{\nu=1}\rangle=|\uparrow\uparrow\uparrow\uparrow\uparrow\uparrow\uparrow\uparrow\uparrow\cdots\uparrow\rangle|\Psi_S\rangle. \tag{3}$$

Finite-size exact diagonalization calculations[14–16] can be used to establish that these conclusions remain valid for the realistic case of Coulomb interactions.

The simplest neutral excitations of the ferromagnetic ground state are those with a single reversed spin. It turns out that it is possible to analytically solve for the wave functions and eigenenergies of these excited states.[17,18] The normalized eigenstates may be labeled by a wave vector $\vec{k}$, and in second quantized notation are given by

$$|\vec{k}\rangle=\frac{1}{\sqrt{N}}\sum_q e^{-iqk_x l_c^2} c^\dagger_{q,\downarrow} c_{q+k_y,\uparrow}|\Psi_{\nu=1}\rangle. \tag{4}$$

The operator relating this state to the ground state is proportional to the Fourier transform of the projection of the spin-lowering operator onto the lowest Landau level, $|\vec{k}\rangle = e^{k^2 l_c^2/4}\overline{S^-}(\vec{k})|\Psi_{\nu=1}\rangle/\sqrt{N}$, where $\overline{S^-}(\vec{k})$ is $S^-(\vec{k})=S^x(\vec{k})-iS^y(\vec{k})$ projected onto the LLL. These states appear to be similar to the single-magnon states of a localized-spin ferromagnet, but there is an important distinction, which is most easily explained by considering a finite-size system. The dimension of the $S^z=N/2-1$ subspace is $N_\phi^2=N^2$, since there are N possible states for the minority-spin electron and N possible states for the majority-spin hole. It is possible to show[19] that for a finite-size quantum Hall system, the number of inequivalent values of the wave vector $\vec{k}$ is also N^2. Since there is one wave vector for each state and translational invariance decouples states with different wave vectors, the eigenstates can be constructed by symmetry arguments alone. This should be contrasted with the case of localized spin Heisenberg ferromagnets for which single-spin-flip states can also be constructed by symmetry arguments alone, but the number of such states is only N. The much larger number of states in the present problem occurs because of the possibility in itinerant electron systems of changing the orbital occupied by an electron whose spin has been reversed.

The nature of the single-spin-flip excitations of quantum Hall ferromagnets gradually changes from having collective spin-wave character at long wavelengths to having single-particle character at larger wave vectors.[18,20] This property is reflected by the dispersion relation[17,18] for single-spin-flip states,

$$\epsilon_{SW}(\vec{k})=\Delta_z+\lambda[\tilde{a}(0)-\tilde{a}(\vec{k})], \tag{5}$$

where the quantity[21]

$$\tilde{a}(\vec{k})=\int \frac{d^2\vec{q}}{(2\pi)^2}\tilde{V}(\vec{q})e^{-(q^2 l_c^2/2)}e^{i[\vec{q}\cdot(\hat{z}\times\vec{k})]l_c^2}. \tag{6}$$

Equation (6) is easy to understand.[18] It represents the attractive interaction between a minority-spin electron and a majority-spin hole, quantum mechanically smeared over their respective cyclotron orbits, and separated in real space

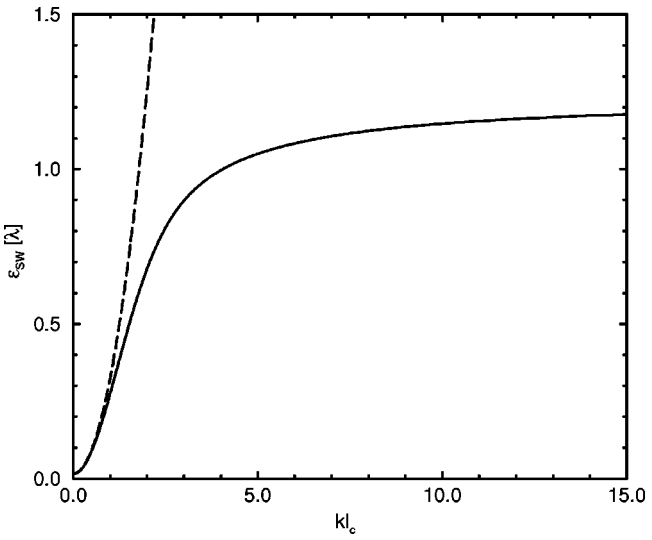

FIG. 1. Spin-wave dispersion $\epsilon_{SW}(k)$ at zero temperature, with a Zeeman gap $\Delta_z = 0.016\lambda$ and a static screening wave vector $k_{sc} = 0.01 l_c^{-1}$. Note the small value of Δ_z compared with the spin-wave bandwidth $\lambda\tilde{a}(0)$. The dashed line shows $\Delta_z + 4\pi\rho_s k^2 l_c^2$.

by $l_c^2 \hat{z}\times\vec{k}$. The attractive interaction contributes negatively to the excitation energy. This magnetoexcitonic picture of spin-flip excitations is especially appropriate when the electron-hole separation exceeds the cyclotron orbit size, i.e., when $l_c|\vec{k}| > 1$. We use this picture in Sec. IV to interpret our result for the interaction between electrons and spin waves. The gap for creating infinitely separated electron-hole pairs, $\Delta_z + \lambda\tilde{a}(0)$, is associated with the incompressible[22] property of quantum Hall states. The property $\epsilon_{SW}(\vec{k}\to 0) = \Delta_z$ is required by spin-rotation invariance of the interaction Hamiltonian. For small k the excitations are collective in character, and

$$\epsilon_{SW}(\vec{k}) = \Delta_z + 4\pi\rho_s l_c^2 k^2, \tag{7}$$

where $\rho_s = \lim_{k\to 0}\lambda[\tilde{a}(0) - \tilde{a}(\vec{k})]/(4\pi l_c^2 k^2)$ is the spin-stiffness parameter, which appears in field theory phenomenologies. In Fig. 1 we plot $\epsilon_{SW}(\vec{k})$ and the above long-wavelength approximation for the case of a weakly screened Coulomb interaction.

The elementary charged excitations of the $|\Psi_{\nu=1}\rangle$ are also known exactly:

$$\begin{aligned} |k\rangle_e &= c^\dagger_{k,\downarrow}|\Psi_{\nu=1}\rangle, \\ |k\rangle_h &= c_{k,\uparrow}|\Psi_{\nu=1}\rangle. \end{aligned} \tag{8}$$

These single Slater determinant states are the maximally spin-polarized states with $N = N_\phi \pm 1$, and have energies $E = E_{\nu=1} + \mu + \xi^{HF}_\downarrow$ and $E = E_{\nu=1} - \mu - \xi^{HF}_\downarrow$, respectively. Explicit expressions for the Hartree-Fock energies are given in Sec. III. Recently it has become clear that for systems with weak Zeeman energies, charged Skyrmion[23] excitations can have lower energies than these states. However, as we discuss below, Skymion states will have little spectral weight in the one-particle Green's function.

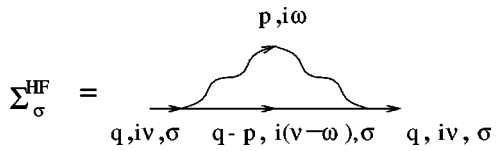

FIG. 2. Proper self-energy diagram in the self-consistent HF approximation. The propagator line in this diagram must be determined self-consistently. This approximation leads to a frequency-independent self-energy, and hence to a Green's function whose spectral weight consists of a single δ function. The first-order tadpole diagram is absent because of the introduction of a neutralizing background charge.

III. HARTREE-FOCK APPROXIMATION AND SHORTCOMINGS OF THE BAND THEORY OF ITINERANT ELECTRON FERROMAGNETISM

In anticipation of subsequent sections we discuss the Hartree-Fock approximation using the lexicon of the imaginary-time thermodynamic Green's-function technique.[24–26] When only the one-particle Zeeman term is retained in Eq. (1), the thermal Green's function $\mathcal{G}^{(0)}$ is given by

$$\mathcal{G}^{(0)}_\sigma(i\nu_n) = \frac{1}{i\hbar\nu_n - \xi^{(0)}_\sigma}, \tag{9}$$

where $\nu_n = (2n+1)\pi/(\hbar\beta)$ is a fermion Matsubara frequency, $\beta = 1/k_B T$, and $\xi^{(0)}_\sigma = -\sigma\Delta_z/2 - \mu$ ($\sigma = +1$ for $\uparrow$, $\sigma = -1$ for $\downarrow$) is the single-particle energy measured from the chemical potential. In the strong-magnetic-field limit, translational invariance implies[27] not only that the Green's function is diagonal in the momentum labels of the Landau gauge states, but also that the diagonal elements are independent of momentum. This general property leads to thermodynamic Green's functions, which depend only on Matsubara frequency and spin.

In the diagram sum we use to approximate the electronic self-energy in Sec. IV. The propagators which appear are self-consistent Hartree-Fock (SHF) propagators rather than the bare propagators of Eq. (9). The Hartree-Fock propagators are obtained by self-consistently solving the Dyson equation with the lowest-order self-energy diagram illustrated in Fig. 2. This leads to an algebraic equation for the self-energy:

$$\Sigma^{HF}_\sigma = \xi^{HF}_\sigma - \xi^{(0)}_\sigma = -\lambda\tilde{a}(0) n_F(\xi^{HF}_\sigma). \tag{10}$$

The SHF Green's function is

$$\mathcal{G}^{HF}_\sigma(i\nu_n) = \frac{1}{i\hbar\nu_n - \xi^{HF}_\sigma}. \tag{11}$$

Since the chemical potential at $\nu = 1$ is determined by the equation $n_F(\xi_\uparrow) + n_F(\xi_\downarrow) = 1$, it follows that $\xi^{HF}_\uparrow(T) = -\xi^{HF}_\downarrow(T) < 0$, and that the chemical potential is fixed at $\mu = -\lambda\tilde{a}(0)/2$ *independent* of temperature and Zeeman energy. For $k_B T < \lambda\tilde{a}(0)/4$ and weak Zeeman coupling it can happen that Eq. (10) has three solutions. In this case we choose the lowest value of $\xi^{HF}_\uparrow$, since this is the solution which minimizes the grand potential (Ω

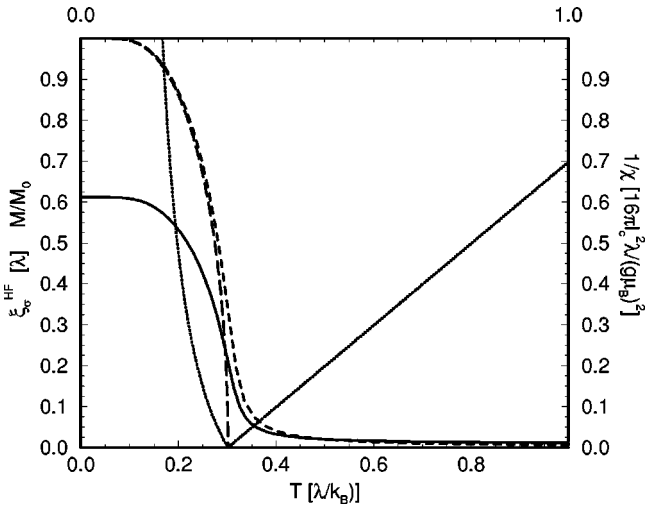

FIG. 3. Hartree-Fock eigenenergy $\xi_{\downarrow}^{HF}$ (solid line) as a function of temperature at $\nu=1$; $\xi_{\uparrow}^{HF}=-\xi_{\downarrow}^{HF}$, because of particle-hole symmetry at $\nu=1$. The magnetization $M=M_0(\nu_{\uparrow}-\nu_{\downarrow})$ within the SHF is depicted for $\Delta_z=0.016\lambda$ (dashed curve) and $\Delta_z=0.0\lambda$ (long dashed curve), respectively. Note the finite magnetization at low T in the latter case, incorrectly indicating the existence of an ordered phase for T below $T_c=\tilde{a}(0)\lambda/(4k_B)$. The uniform static inverse susceptibility is plotted as a dotted line in units of $(16\pi l_c^2\lambda)/(g\mu_B)^2$ for $T\geqslant T_c$, as well for $T<T_c$.

$=-2Nk_BT\ln[2\cosh(\beta\xi_{\uparrow}/2)]$. In Fig. 3 we plot the Hartree-Fock eigenvalue $\xi_{\downarrow}^{HF}$ and the spin magnetization as a function of temperature. The difference $\xi_{\downarrow}^{HF}-\xi_{\uparrow}^{HF}=2\xi_{\downarrow}^{HF}$ is the exchange enhanced spin splitting[28,29] of the lowest Landau level. Its maximum value occurs at $T=0$ and is $\tilde{a}(0)\lambda+\Delta_z$, dominated by the interaction term for $\Delta_z\ll\lambda$. In the high-temperature limit ($T\to\infty$) this gap reduces to the bare Zeeman splitting Δ_z.

The sharp inflection point in the spin magnetization curve for $\Delta_z=0.016\lambda$ in Fig. 3 is a remnant of the spontaneous magnetization that occurs *incorrectly* in the SHF Green's function at low temperatures. For $\nu=1$ and $\Delta_z=0$ it follows from Eq. (10) that $x\equiv\beta\xi_{\uparrow}^{HF}$ satisfies

$$x=\beta\tilde{a}(0)\lambda\left(\frac{1}{2}-\frac{1}{(e^x+1)}\right). \tag{12}$$

At high temperatures the only solution to this equation is $x=0$ so that $n_F(\xi_{\uparrow}^{HF})=n_F(\xi_{\downarrow}^{HF})=1/2$ and there is no spin polarization. Expanding the right-hand side of Eq. (12), we see that $x\neq 0$ solutions are possible when the coefficient of the linear term exceeds 1, i.e., for $T<T_c^{HF}=\tilde{a}(0)\lambda/(4k_B)$. Expanding Eq. (12) up to third order, we find the expected mean-field behavior for T near T_c^{HF}:

$$\frac{M(T)}{M(T=0)}=\sqrt{3}\frac{T}{T_c^{HF}}\left(1-\frac{T}{T_c^{HF}}\right)^{1/2}. \tag{13}$$

Similarly, at T_c^{HF} we obtain

$$\frac{M(T=T_c^{HF},\Delta_z)}{M(T=0)}=\left(\frac{3\Delta_z}{\tilde{a}(0)\lambda}\right)^{1/3}, \tag{14}$$

with mean field exponent $\delta=3$. The SHF spontaneous magnetization is plotted in Fig. 3.

The finite T ferromagnetic instability of the SHF Green's function also appears in the random-phase-approximation (RPA) expression for the spin susceptibility per area $\overline{\chi}^{-+}(\vec{q},i\omega_n)=1/\hbar\int_0^{\hbar\beta}d\tau\, e^{i\omega_n\tau}\overline{\chi}^{-+}(\vec{q},\tau)$, where $\omega_n=2n\pi/(\hbar\beta)$ are bosonic Matsubara frequencies and

$$\overline{\chi}^{-+}(\vec{q},\tau)=\frac{(g\mu_B)^2}{A}\langle T\overline{S}^{-}(\vec{q},\tau)\overline{S}^{+}(-\vec{q},0)\rangle. \tag{15}$$

The overbar is intended to emphasize that the susceptibility is to be evaluated in the strong-field limit, where the Hamiltonian can be projected onto the LLL. The RPA expression can be obtained from a ladder diagram sum with SHF Green's functions, similar to the sum for the self-energy detailed in Sec. IV. The result is[30]

$$\begin{aligned}\overline{\chi}^{-+(RPA)}(\vec{q},i\omega_n)&=\frac{\overline{\chi}^{-+(HF)}(\vec{q},i\omega_n)}{1+I(\vec{q})\overline{\chi}^{-+(HF)}(\vec{q},i\omega_n)}\\&=\frac{(g\mu_B)^2e^{-q^2l_c^2/2}}{2\pi l_c^2}\frac{(\nu_{\uparrow}^{HF}-\nu_{\downarrow}^{HF})}{[i\hbar\omega_n+\tilde{\epsilon}_{SW}(\vec{q})]}\end{aligned} \tag{16}$$

where the single-bubble HF spin susceptibility

$$\overline{\chi}^{-+(HF)}(\vec{q},i\omega_n)=\frac{(g\mu_B)^2e^{-q^2l_c^2/2}}{2\pi l_c^2}\frac{(\nu_{\uparrow}^{HF}-\nu_{\downarrow}^{HF})}{(i\hbar\omega_n-\xi_{\uparrow}^{HF}+\xi_{\downarrow}^{HF})} \tag{17}$$

is the bubble with HF lines. The effective interaction appearing in Eq. (16) is defined by $I(\vec{q})=-2\pi l_c^2/(g\mu_B)^2e^{q^2l_c^2/2}\tilde{a}(\vec{q})\lambda$. The quantity $\tilde{\epsilon}_{SW}(\vec{q})$,

$$\tilde{\epsilon}_{SW}(\vec{q})=\Delta_z+\lambda(\nu_{\uparrow}^{HF}-\nu_{\downarrow}^{HF})[\tilde{a}(0)-\tilde{a}(\vec{q})], \tag{18}$$

reduces to the spin-wave spectrum $\epsilon_{SW}(\vec{q})$ of Eq. (5) in the $T\to 0$ limit. In this approximation, the spin-wave bandwidth is reduced in proportion to the spin polarization as the temperature increases. Note that this approximation does not capture the finite lifetime of spin-wave–states, which will result from spin-wave spin-wave interactions at higher temperatures. This will be one of the important limitations of the theory we present in Sec. IV.

For $\Delta_z=0$ the static limit of the RPA susceptibility, plotted in Fig. 3, diverges at the same temperature at which the spontaneous magnetization determined by the SHF equations (10) vanishes. These results are in disagreement with the Mermin-Wagner theorem, which forbids continuous broken symmetries at finite temperatures in two dimensions. The disagreement is expected for mean-field theory. It clear that the SHF magnetizations calculated at relatively small but finite values of Δ_z, appropriate for experimental systems, will be too large. In essence, the SHF calculations of this section are equivalent to the Stoner band theory[3,31] of metallic ferromagnetism. In both cases the ground state is well described. (In the present situation the SHF ground state and the exact ground state are identical.) In both cases the magnetization is overestimated at finite temperatures primarily

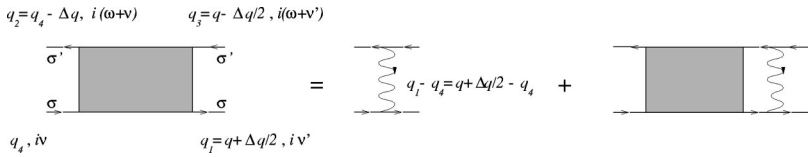

FIG. 4. The self-consistent integral equation for the scattering vertex $\Gamma^{(4)}$ in the particle-hole ladder approximation.

because of the failure to account for magnetization suppression due to thermally excited collective spin-wave excitations. The approximation discussed in Sec. IV remedies this gross deficiency. The situation in the present two-dimensional systems with a small Zeeman coupling is not unlike the situation in most three-dimensional metallic ferromagnets with no external field. For example it is generally accepted[32] that most but not all of the magnetization suppression up to the critical temperature in the elemental metallic ferromagnets (Fe, Ni, and Co) is due to spin-wave excitations. Of course, the separation of magnetization suppression into collective spin-wave effects and the particle-hole effects cannot, in general, be made precise. In metallic ferromagnets, and in the present two-dimensional systems, a complete theory valid at moderately high temperatures requires the interplay between collective spin fluctuations and the underlying fermionic degrees of freedom to be accurately described. Section IV reports on an adaptation of microscopic theories of metallic ferromagnets to the present case.

IV. ELECTRON SPIN-WAVE SCATTERING

Our theory is based on an expansion in terms of SHF Green's functions. The self-energy correction to these propagators can in principle be expressed in terms of the exact scattering vertex $\Gamma^{(4)}(1,2,3,4)$ and the exact GF. [Here 1 is short for $(q_1, i\nu_{1,n})$.] We use an approximation, which, as we shall demonstrate, captures much of the essential physics. It is the analog for quantum Hall ferromagnets of the approximation discussed by Hertz and Edwards[33] for the case of single-band Hubbard models with ground states, which are strong ferromagnets. The self-energy is approximated by a particle-hole ladder summation, which gives an exact description of interactions between a single hole in the majority band and a single electron in the minority band. However, as the density of spin-flip excitations increases at higher temperatures, the approximation becomes less accurate.

The Bethe-Salpeter integral equation for the scattering vertex is expressed diagrammatically in Fig. 4. Explicit calculation of low-order ladder-diagram particle-hole vertex parts using Feynman rules shows that, in this approximation,

$$\Gamma^{(4)}(1,2,3,4)=\Gamma^{(4)}(q+\Delta q/2-q_4,\Delta q;i\omega_n) \tag{19}$$

depends only on two momenta and one frequency. Here $q=(q_1+q_3)/2$ and $\Delta q=q_1-q_3$ are the center-of-mass and the relative momenta, respectively, and $i\omega_n=i(\nu_{3,n}-\nu_{1,n})$ is the bosonic Matsubara frequency of the relative motion of the ingoing and outgoing particles.

The Bethe-Salpeter integral equation for the scattering vertex is

$$\begin{aligned}\Gamma^{(4)}_{\sigma,\sigma'}(q+\Delta q/2-q_4,\Delta q;i\omega_n)&=\lambda\tilde{W}(q+\Delta q/2-q_4,\Delta q)+\lambda\overline{\chi}_{\sigma,\sigma'}(i\omega_n)l_c\\&\times\int_{-\infty}^{\infty}dq'\tilde{W}(q-q',\Delta q)\\&\times\Gamma^{(4)}_{\sigma,\sigma'}(q'+\Delta q/2-q_4,\Delta q;i\omega_n).\end{aligned} \tag{20}$$

Here we have introduced the pair propagator $\overline{\chi}_{\sigma,\sigma'}(i\omega_n)$, defining

$$\overline{\chi}_{\sigma,\sigma'}(i\omega_n)=-\frac{1}{\beta}\sum_{i\nu_n}\mathcal{G}_\sigma(i\nu_n)\mathcal{G}_{\sigma'}[i(\nu_n+\omega_n)]. \tag{21}$$

It is important to note that the q independence of the GF in the case of quantum Hall ferromagnets immensely simplifies the solution of the Bethe-Salpeter equation. In fact, Eq. (20) can be reduced to an algebraic equation because the second term on the right-hand side is a convolution integral in the center of mass coordinate.[18] We define a partial Fourier transformation of the scattering function:

$$\begin{aligned}\tilde{\Gamma}^{(4)}_{\sigma,\sigma'}(p,\Delta q;i\omega_n)&=l_c\int_{-\infty}^{\infty}dqe^{ipql_c^2}\Gamma^{(4)}_{\sigma,\sigma'}(q,\Delta q;i\omega_n)\\&=e^{ip(\Delta q/2-q_4)l_c^2}l_c\int_{-\infty}^{\infty}dqe^{ipql_c^2}\\&\times\Gamma^{(4)}_{\sigma,\sigma'}(q+\Delta q/2-q_4,\Delta q;i\omega_n).\end{aligned} \tag{22}$$

The corresponding transformation of the Landau-gauge vertex $\tilde{W}(q,\Delta q)$ is the particle-hole interaction, which appeared previously in Eq. (18),

$$\begin{aligned}\tilde{a}(\vec{k}=(\Delta q,p))&=l_c\int_{-\infty}^{\infty}dqe^{ipql_c^2}\tilde{W}(q,\Delta q)\\&=\int\frac{d^2\vec{q}'}{(2\pi)^2}\tilde{V}(\vec{q}')e^{-q'^2l_c^2/2}e^{i(q'_x\Delta q+q'_yp)l_c^2},\end{aligned} \tag{23}$$

where we have defined the two-dimensional wave vector $\vec{k}=(\Delta q,p)$. With these definitions we find that

$$\tilde{\Gamma}^{(4)}_{\sigma,\sigma'}[\vec{k}=(p,\Delta q);i\omega_n]=\frac{\tilde{a}(\vec{k})\lambda}{[1-\overline{\chi}_{\sigma,\sigma'}(i\omega_n)\tilde{a}(\vec{k})\lambda]}. \tag{24}$$

Our self-energy approximation consists of combining this scattering vertex with the propagators. In order to avoid double counting the first-order terms already present in the Hartree-Fock propagators, we must subtract the first order term from the right-hand side of Eq. (24). Inverting the trans-

form of Eq. (22) then gives the sum of second- and higher-order terms in the Bethe-Salpeter equation. The approximate self-energy for spin σ is obtained by contracting the incoming and outgoing lines of the opposite spin into a Hartree-Fock propagator. The result is that

$$\tilde{\Sigma}_\sigma(i\nu_n)=\frac{1}{\beta}\sum_{i\omega_n}\mathcal{G}_{\sigma'}[i(\nu_n+\omega_n)]\tilde{\Gamma}^{(4)}_{\sigma,\sigma'}(i\omega_n), \qquad (25)$$

where

$$\begin{aligned}\tilde{\Gamma}^{(4)}_{\sigma,\sigma'}(i\omega_n)&\equiv 2\pi l_c^2\int\frac{d^2\vec{k}}{(2\pi)^2}\,\tilde{\Gamma}^{(4)}_{\sigma,\sigma'}(\vec{k};i\omega_n)\\&=2\pi l_c^2\int\frac{d^2\vec{k}}{(2\pi)^2}\\&\quad\times\left\{\frac{\tilde{a}(\vec{k})\lambda}{[1-\overline{\chi}_{\sigma,\sigma'}(i\omega_n)\tilde{a}(\vec{k})\lambda]}-\tilde{a}(\vec{k})\lambda\right\}.\end{aligned} \qquad (26)$$

The Dyson equation relating the SHF and full Green's function is

$$[\mathcal{G}_\sigma(i\nu_n)]^{-1}-[\mathcal{G}^{HF}_\sigma(i\nu_n)]^{-1}=-\tilde{\Sigma}_\sigma(i\nu_n). \qquad (27)$$

Below we address the question of whether the SHF Green's function or the corrected Green's function should be used in the expression for the pair propagator. If we use SHF Green's functions, the particle-hole ladder diagram of order n is proportional to $(\nu^{HF}_\sigma-\nu^{HF}_{\sigma'})^{(n-1)}$. At low temperature this factor is close to 1 and larger than the combinations of filling factors, which result from other diagrams of the same order. For instance, the corresponding particle-particle ladder is proportional to $(1-\nu^{HF}_\sigma-\nu^{HF}_{\sigma'})^{(n-1)}$, which is zero for any T when $\sigma\neq\sigma'$. This observation may be used at low temperatures to systematically justify the class of diagrams we have included. At higher temperatures we expect that the sums of ring diagrams, which describe screening physics[34] will be among the important omissions.

It is possible to require that the Green's functions used in the pair-propagator and self-energy expressions be obtained from the Dyson equation. This leads to a set of coupled equations, which can be solved numerically. For this purpose it is convenient[10] to express the equations in the following mixed imaginary-time imaginary-frequency representation:

$$\begin{aligned}&\mathcal{G}^{-1}_\sigma(i\nu_n)-[\mathcal{G}^{HF}_\sigma(i\nu_n)]^{-1}=-\tilde{\Sigma}_\sigma(i\nu_n),\\&\tilde{\Sigma}_\sigma(\tau)=\tilde{\Gamma}^{(4)}_{\sigma,\sigma'}(-\tau)\mathcal{G}_{\sigma'}(\tau),\\&\tilde{\Gamma}^{(4)}_{\sigma,\sigma'}(i\omega_n)=2\pi l_c^2\int\frac{d^2\vec{k}}{(2\pi)^2}\\&\quad\times\left\{\frac{\tilde{a}(\vec{k})\lambda}{(1-\overline{\chi}_{\sigma,\sigma'}(i\omega_n)\tilde{a}(\vec{k})\lambda)}-\tilde{a}(\vec{k})\lambda\right\},\\&\overline{\chi}_{\sigma,\sigma'}(\tau)=-\mathcal{G}_\sigma(-\tau)\mathcal{G}_{\sigma'}(\tau)\end{aligned} \qquad (28)$$

As we discuss below, we have found that these self-consistent equations tend not to have stable solutions at low temperature.

Our work is based mainly on the approximation in which the pair propagator and the self-energy are evaluated with SHF Green's functions. The pair-propagator frequency sum may then be evaluated analytically,

$$\overline{\chi}^{HF}_{\sigma,\sigma'}(i\omega_n)=-\frac{[n_F(\xi^{HF}_\sigma)-n_F(\xi^{HF}_{\sigma'})]}{(i\hbar\omega_n+\xi^{HF}_\sigma-\xi^{HF}_{\sigma'})}, \qquad (29)$$

leading to the following explicit expressions for the corrections $\tilde{\Sigma}_\sigma(i\omega_n)$ of the majority- spin and minority-spin SHF self-energies:

$$\begin{aligned}\tilde{\Sigma}_\uparrow(i\nu_n)&=\lambda^2(\nu^{HF}_\uparrow-\nu^{HF}_\downarrow)\int_0^\infty d\left(\frac{k^2l_c^2}{2}\right)\tilde{a}^2(k)\\&\quad\times\frac{\{n_B[\tilde{\epsilon}_{SW}(k)]+n_F(\xi^{HF}_\downarrow)\}}{[i\hbar\nu_n+\tilde{\epsilon}_{SW}(k)-\xi^{HF}_\downarrow]}\end{aligned} \qquad (30)$$

and

$$\begin{aligned}\tilde{\Sigma}_\downarrow(i\nu_n)&=\lambda^2(\nu^{HF}_\uparrow-\nu^{HF}_\downarrow)\int_0^\infty d\left(\frac{k^2l_c^2}{2}\right)\tilde{a}^2(k)\\&\quad\times\frac{\{n_B[\tilde{\epsilon}_{SW}(k)]+1-n_F(\xi^{HF}_\uparrow)\}}{[i\hbar\nu_n-\tilde{\epsilon}_{SW}(k)-\xi^{HF}_\uparrow]}.\end{aligned} \qquad (31)$$

Here $n_B[\tilde{\epsilon}_{SW}(k)]$ is the Bose-Einstein distribution function for the spin-waves whose dispersion is specified in Eq. (18). For $T=0$ the occupation factors in the numerators of both self-energy expressions vanish, and the SHF result, which is exact in this limit, is recovered.

These electronic self-energy expressions resemble those due to virtual phonon exchange in an electron-phonon system.[26] The majority-spin self-energy includes contributions from processes where a majority-spin electron scatters out to a minority-spin state upon absorption of a spin wave, and processes where a minority-spin electron scatters into a majority-spin state upon emission of a spin wave. Because the spin wave carries spin $S_z=-1$, there are no processes where a majority-spin electron scatters to a minority-spin state and emits a spin wave or a minority-spin electron scatters to a majority-spin state and absorbs a spin wave. This distinction explains both the difference between the majority-spin self-energy in Eq. (30) and the minority-spin self-energy in Eq. (31) and the difference between these self-energies and the phonon exchange self-energy where both classes of contribution appear at once.[26] The electron self-energy expressions are identical to those which would be obtained for a model where the electrons and spin waves were regarded as independent fermion and boson particles with an interaction in which fermions are scattered by emitting or absorbing spin waves. The effective electron spin-wave interaction, which can be read off from the self-energy expressions, is proportional to $\lambda\tilde{a}(\vec{k})$. Note that, unlike the case of deformation potential electron-phonon coupling, the matrix element approaches a constant as $k\to 0$. If the long-range Coulomb interaction is not screened, the electron spin-

wave interaction falls off only as $|k|^{-1}$ for large k. [For ideal 2D Coulomb interactions $\tilde{a}(\vec{k})=\sqrt{\pi/2}e^{-k^2l_c^2/4}I_0(k^2l_c^2/4)$.] The electron spin-wave interaction at large k can be understood in terms of the excitonic picture discussed in Sec. II and is proportional to the electron-electron interaction at *real-space* separation kl_c^2. If the Coulomb interaction is screened $\tilde{a}(\vec{k})$ will begin to fall off more quickly once kl_c^2 exceeds $\sim k_{sc}^{-1}$. The slow falloff of these large momentum-transfer scattering events requires us to take account of screening when we evaluate the self-energy expressions.

Note that these self-energy expressions satisfy the equation $\tilde{\Sigma}_\uparrow(i\nu_n)=-\tilde{\Sigma}_\downarrow(-i\nu_n)$. This is an exact identity for the case $\nu=1$, which follows from the particle-hole symmetry[35] of the underlying Hamiltonian. We remark that the self-energies given by Eqs. (30) and (31) have branch cuts along a finite portion of the real line. For majority spins the branch cut occurs along the interval $I_\uparrow=(\xi_\uparrow^-=\xi_\uparrow^{HF},\xi_\uparrow^+=\xi_\downarrow^{HF}-\Delta_z)$. For the minority spin the branch cut interval is $I_\downarrow=(\xi_\downarrow^-=\xi_\uparrow^{HF}+\Delta_z,\xi_\downarrow^+=\xi_\downarrow^{HF})$. Outside of these intervals the self-energy is real on the real line. Because of the branch cuts, some care is required in the numerical evaluation of the self-energy expression.

In this paper we concentrate on physical properties which can be expressed in terms of the one-particle real-time Green's function. Analytically continuing the thermal Green's function self-energy expressions [Eqs. (30) and (31)], to the real frequency axis ($i\hbar\nu_n\rightarrow E+i\eta$) gives $G_\sigma^{ret}(E)=1/[E+i\eta-\xi_\sigma^{HF}-\tilde{\Sigma}_\sigma(E)]$. The retarded Green's function is completely specified by its spectral function

$$A_\sigma(E)=-2\,\mathrm{Im}\,G_\sigma^{ret}(E). \tag{32}$$

It is $A_\sigma(E)$, which we evaluate numerically, and we start by mentioning some of its general properties. If we consider the system of equations defining the SHF GF equation (28) and start the iteration from the bottom equation with a GF satisfying $\mathcal{G}_\uparrow(i\nu_n)=-\mathcal{G}_\downarrow(-i\nu_n)$, we end up with a GF satisfying the same relation, i.e., the approximate system of equations conserves this property. The SHF GF has this property since $\xi_\downarrow^{HF}=-\xi_\uparrow^{HF}$. Since $G_\uparrow^{ret}(E)=-G_\downarrow^{av}(-E)$, the spectral functions for up- and down-spins satisfy the following relationship:

$$A_\uparrow(E)=A_\downarrow(-E). \tag{33}$$

Therefore, the knowledge of the spectral function for only one spin direction for the case of $\nu=1$ is sufficient to determine the result for the other spin directions.

When the self-energy is evaluated from the Hartree-Fock GF the qualitative behavior of $A_\uparrow(E)$ can be understood from the analytical structure of the denominator $[E-\xi_\uparrow^{HF}-\tilde{\Sigma}_\uparrow(E)]$ of the GF. The spectral function for $\sigma=\uparrow$ is nonzero along the branch cut where the retarded self-energy has a nonzero imaginary part, i.e., for $\xi_\uparrow^{HF}\leq E\leq\xi_\downarrow^{HF}-\Delta_z$. Since the real part of the self-energy is monotonically decreasing outside of this interval, it vanishes for $E\rightarrow\pm\infty$, and is divergent for $E\rightarrow\xi_\downarrow^{HF}-\Delta_z$ from above (see below), it follows that the Green's function also has simple poles, and the spectral function has δ-function contributions on both sides of the branch cut. The positions of these quasiparticle poles in the Green's function are determined by

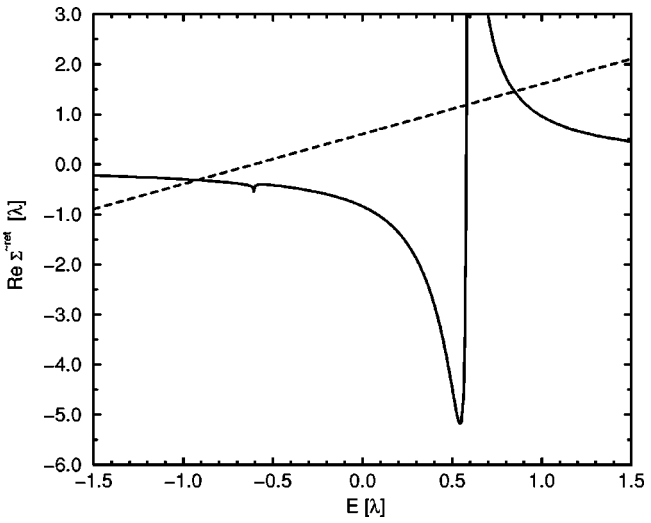

FIG. 5. The real part of the self-energy $\tilde{\Sigma}_\uparrow^{ret}(E)$ and the line $E-\xi_\uparrow^{HF}$ as functions of E at temperature $T=0.1\lambda/k_B(\Delta_z=0.016\lambda, k_{sc}=0.01l_c^{-1}, w=0.0l_c)$. The quasiparticle poles occur at the two energy values $E_\uparrow^-$ and $E_\uparrow^+$, at which the curves intersect. Because the self-energy diverges in opposite directions as the upper and lower boundaries of the central branch-cut interval, two poles exist at any temperature in this approximation.

$$E-\xi_\sigma^{HF}=\tilde{\Sigma}_\sigma^{ret}(E). \tag{34}$$

Figure 5 illustrates a graphical solution of this equation for $T=0.1\lambda/k_B$. As we discuss below, the spectral weight is dominated by the two δ-function contributions at E_σ^- and E_σ^+ except at elevated temperatures.

To obtain a qualitative feel for the physics of the self-energy at low temperatures, it is useful to divide it into separate contributions from interactions with collective long-wavelength spin waves and from interactions with short wavelength spin-down electron, spin-up hole pairs. We arbitrarily treat spin waves with $kl_c<1$ as collective, and those with $kl_c>1$ as single particle. For collective spin waves we can approximate the electron-spin-wave interaction by a constant $\lambda\tilde{a}(0)$, and the low-energy spin-wave dispersion by $\Delta_z+4\pi\rho_s l_c^2k^2$. Similarly, for particle-hole states we can, when screening is neglected, approximate the interaction by λ/kl_c and the spin-wave energy by $2\xi_\downarrow^{HF}-\lambda/kl_c$. We first concentrate on the region of energy E near $\xi_\uparrow^{HF}$, where the main spectral weight resides at low temperatures. The collective spin-wave contribution to the self-energy near the low-energy quasiparticle is

$$\tilde{\Sigma}_\uparrow^{C-}(E)\approx-[\lambda\tilde{a}(0)l_c]^2\int_0^{l_c^{-1}}dkk\frac{n_B[\epsilon_{SW}(k)]}{\lambda\tilde{a}(0)+\xi_\uparrow^{HF}-E}. \tag{35}$$

We have assumed here that the spin-wave Bose factor is larger than the spin-down electron Fermi factor. Note that this requires, at a minimum, that Δ_z be less than *half* the single-particle energy gap $\xi_\downarrow^{HF}-\xi_\uparrow^{HF}$. The extra factor of 2 in this condition occurs because of the itinerant nature of the

single-particle excitations. This self-energy contribution will be negative and only weakly energy dependent for $E < \xi_{\uparrow}^{HF}$. The particle-hole contribution to the self-energy in the same energy range is

$$\tilde{\Sigma}_{\uparrow}^{PH-}(E) \approx -\lambda^2 \int_{l_c^{-1}}^{\infty} dk k^{-1} \frac{n_F(\xi_{\downarrow}^{HF})}{\xi_{\uparrow}^{HF} + \lambda/k l_c - E}. \quad (36)$$

This contribution to the self-energy is sharply energy dependent, reaching a maximum for $E = \xi_{\uparrow}^{HF}$, and is formally divergent for every energy. The divergence comes from the large-k contribution to the integral, i.e., from the interaction of electrons with widely separated spin-flip electron-hole pairs. It can be cured by introducing screening into our theory as discussed earlier. Screening effectively cuts off the divergent integral at $k \sim 1/k_{sc} l_c^2$. At low T, a Thomas-Fermi approximation estimate would give $k_{sc} l_c \sim \lambda \exp(-\xi_{\downarrow}^{HF}/k_B T)$. The screening wave vector is exponentially small because of the gap for charged excitations, and the ultraviolet cutoff is consequently exponentially large. However, except at $E = \xi_{\uparrow}^{HF}$, the particle-hole self-energy contribution depends only logarithmically on the screening vector, and the declining Fermi factor will result in a small contribution at low temperatures. At $E = \xi_{\uparrow}^{HF}$, the particle-hole contribution depends linearly on k_{sc}^{-1}, leading to a very narrow peak near this energy at low temperatures.

Because of the collective contribution to the self-energy, the low-energy quasiparticle pole will be shifted to energies below $\xi_{\uparrow}^{HF}$ and away from this peak. In the end the particle-hole contribution to the self-energy is much larger than it would be for a system with short-range interactions. Nevertheless, provided that the collective gap Δ_z is much less than half the particle-hole gap, there will be a region at low-temperatures where its contribution becomes unimportant. Neglecting this contribution we find the low-energy pole has a residue

$$z = \left[1 + l_c^2 \int_0^{l_c^{-1}} dk k n_B[\epsilon_{SW}(k)] \right]^{-1}, \quad (37)$$

and occurs at energy

$$E_{\uparrow}^{-} = \xi_{\uparrow}^{HF} - \lambda \tilde{a}(0)[1 - z]. \quad (38)$$

The electron-spin-wave interaction strength drops out of the expression for z because of its relationship to the spin-flip excitation energies. As we discuss below, the loss of spectral weight due to occupied spin waves gives a magnetization suppression identical to that which would be obtained from a noninteracting spin-wave model with appropriate ultraviolet cutoffs.

A similar calculation can be carried out for the high-energy pole in the Green's function. For $E = \xi_{\downarrow}^{HF} - \Delta_z + \delta$ and δ small, we can again identify approximate collective and particle-hole contributions to the self-energy:

$$\tilde{\Sigma}_{\uparrow}^{C+}(E) \approx [\lambda \tilde{a}(0) l_c]^2 \int_0^{l_c^{-1}} dk k \frac{n_B[\epsilon_{SW}(k)]}{\delta + 4\pi\rho_s k^2 l_c^2} \quad (39)$$

and

$$\tilde{\Sigma}_{\uparrow}^{PH+}(E) \approx \lambda \int_{l_c^{-1}}^{\infty} dk k^{-1} \frac{n_F(\xi_{\downarrow}^{HF})}{\tilde{a}(0)}. \quad (40)$$

In this case, screening is not necessary to make the particle-hole contribution small at low temperatures. The second term in the denominator of Eq. (39) is negligible if $\delta \gg k_B T$ because of the exponential cutoff in the spin-wave Bose occupation factors; we see below that the condition is satisfied at the upper pole in the Green's function. Keeping only the collective contribution gives a high-energy pole with residue $z^{+} = z^{-1} - 1$ and energy

$$E_{\uparrow}^{+} = \xi_{\downarrow}^{HF} - \Delta_z + \lambda \tilde{a}(0)[z^{-1} - 1]. \quad (41)$$

For $4\pi\rho_s \gg k_B T \gg \Delta_z$, it follows from Eq. (37) that

$$z^{-1} - 1 = \frac{k_B T}{8\pi\rho_s} \ln(k_B T/\Delta_z). \quad (42)$$

which, since $16\pi\rho_s = \lambda \tilde{a}(0)$, guarantees that δ is in the assumed energy range. The approximations made above fail when $z^{-1} - 1$ is large, in which case the sums of the approximate residues exceeds 1. When $1 - z$ is small, it follows from these calculations that the spectral weight of the Green's function is exhausted by the two poles in the Green's function. As spin waves are excited, weight is shifted from the low-energy pole, which is below the chemical potential, to the high-energy pole, which is above the chemical potential. In the limit of zero temperature, the spectral weight lies entirely in the low-energy pole, and Hartree-Fock theory results are recovered.

As we see from Fig. 5 and from the above discussion, the real part of the self-energy diverges to $-\infty$ at the lower limit of the branch cut when screening is neglected, and to $+\infty$ at its upper limit even if screening is included. The divergence at $E = \xi_{\uparrow}^{HF}$ in Fig. 5 produces only a small feature in our numerical calculations because these results were obtained with $k_{sc} \neq 0$. However, the divergence at the upper boundary of the branch cut is clearly visible. The imaginary part of the GF is nonzero throughout the interval from $\xi_{\uparrow}^{HF}$ to $\xi_{\downarrow}^{HF} - \Delta_z$, because spin-flip excitations exist at all energies between Δ_z and $\Delta_z + \lambda \tilde{a}(0)$. The imaginary part of the retarded Green's function is negative definite, as illustrated in Fig. 6.

The explicit expression for the spectral density is

$$A_{\sigma}(E) = \frac{2\pi\delta(E - E_{\sigma}^{-})}{\left| 1 - \frac{\partial \tilde{\Sigma}_{\sigma}^{ret}(E)}{\partial E} |_{E = E_{\sigma}^{-}} \right|} + \frac{2\pi\delta(E - E_{\sigma}^{+})}{\left| 1 - \frac{\partial \tilde{\Sigma}_{\sigma}^{ret}(E)}{\partial E} |_{E = E_{\sigma}^{+}} \right|} + \theta(E - \xi_{\sigma}^{-})\theta(\xi_{\sigma}^{+} - E) \times \frac{[-2\,\mathrm{Im}\,\tilde{\Sigma}_{\sigma}^{ret}(E)]}{[E - \xi_{\sigma}^{HF} - \mathrm{Re}\,\tilde{\Sigma}_{\sigma}^{ret}(E)]^2 + [\mathrm{Im}\,\tilde{\Sigma}_{\sigma}^{ret}(E)]^2}. \quad (43)$$

The condition that the integral of the spectral function over frequencies equal to one can be used to check the accuracy of our calculations.

We have previously[9] published figures illustrating the spectral densities obtained from numerical evaluations of this

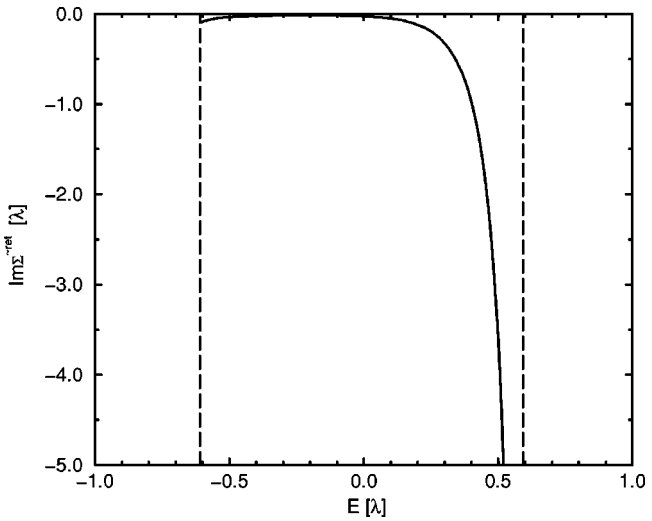

FIG. 6. The imaginary part of the spin-up self-energy $\tilde{\Sigma}_{\uparrow}^{ret}(E)$ at $T=0.1\lambda/k_B$. This quantity is nonzero only within the central interval $I_{\uparrow}$ defined in the text. Note that the imaginary part tends to a finite value on the right boundary of this interval. The parameters are the same as in Fig. 5.

self-energy expression at several temperatures. In agreement with the preceding analysis, the spectrum consists of low- and high-energy δ functions separated by a band associated with the branch cut of the self-energy. The incoherent band contribution to the spectral weight tends to be peaked toward its high-energy extremum where the imaginary part of the self-energy has contributions from long-wavelength spin waves. The spectral weight shifts with increasing temperature from the low-energy Hartree-Fock pole to the high-energy pole and partially to the intermediate-energy band. The spectral weight shift can be understood in terms of a reduction in the probability that majority spins will be lined up with the exchange field from the ordered moment, which fluctuates when spin waves are excited at finite temperatures. In Fig. 7 we plot the fraction of the spectral weight coming

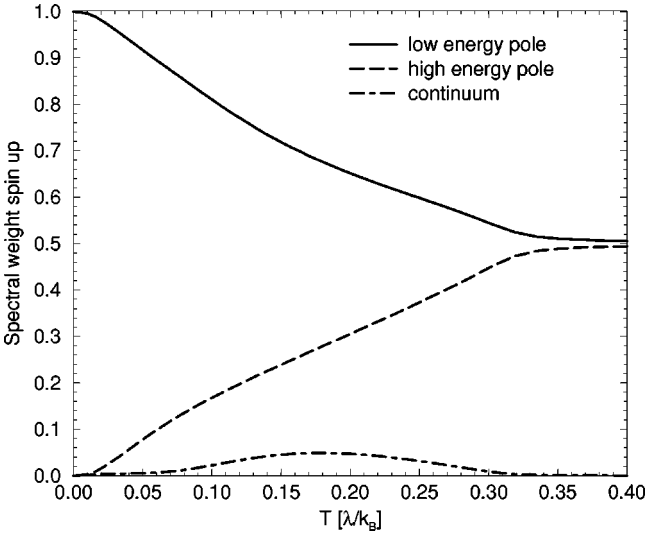

FIG. 7. Temperature dependence of the partitioning of the majority-spin Green's-function spectral weight between low- and high-energy poles, and the intermediate-energy continuum.

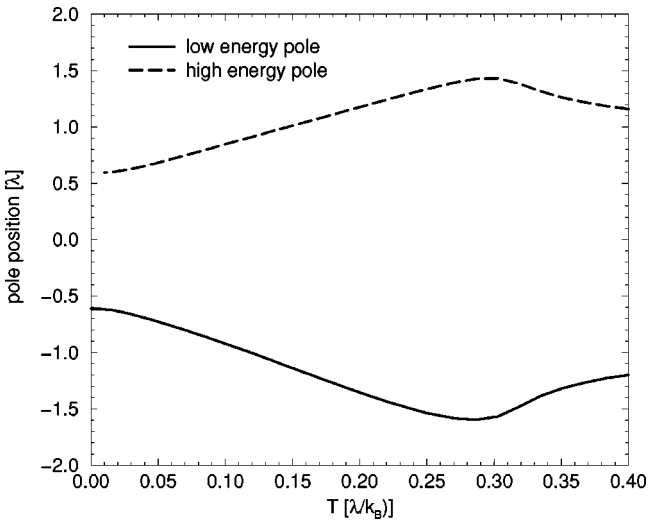

FIG. 8. Positions of the low- and high-energy poles $E_{\uparrow}^{-}$ and $E_{\uparrow}^{+}$ in the majority-spin Green's function $G_{\uparrow}^{ret}(E)$ as a function of temperature ($\Delta_z=0.016\lambda, k_{sc}=0.01l_c^{-1}$, and $w=0.0l_c$).

from these three contributions as a function of temperature. Note that the incoherent band contribution grows rather slowly with temperature. In Fig. 8 we also plot the positions of the two-pole band as a function of temperature. Initially, the two poles are separated by the zero-temperature exchange splitting gap. In the approximation we employ, the splitting increases at finite temperatures because of level repulsion with the continuum states. The results shown in Fig. 8 are for screened interactions between the electrons; accounting for the finite width of the quantum well or heterojunction reduces the splittings to approximately two-thirds of these values for typical systems, and screening associated with Landau level mixing will cause a further reduction.

In Sec. V we discuss several experiments which can test the predictions which result from this spin-wave exchange approximation for the self-energy. Potentially the most telling of these will be 2D-2D tunneling experiments which measure the spectral functions fairly directly. We do not expect perfect agreement between the present theory and experiment, although a qualitative agreement seems certain. We expect that a comparison with tunneling experiments will assist in future theoretical progress. Tunneling spectrum measurements in typical band ferromagnets are much less informative because the bandwidth (which is zero in the present problem) is comparable to the quasiparticle band spin splitting.[36]

V. OBSERVABLES

A. Spin magnetization

The spin magnetization is proportional to the difference of the occupation probabilities for spin-up and -down electrons, $M(T)=M_0(\nu_{\uparrow}-\nu_{\downarrow})$, where $M_0=N|g\mu_B|/2$ is the ground-state spin magnetization. Expressing the occupation probability ν_{σ} in terms of the spectral functions gives

$$\frac{M(T)}{M_0}=\int_{-\infty}^{\infty}\frac{dE}{2\pi}n_F(E)[A_{\uparrow}(E)-A_{\downarrow}(E)]$$

$$=-\int_{-\infty}^{\infty}\frac{dE}{2\pi}\tanh(\beta E/2)A_{\uparrow}(E). \qquad (44)$$

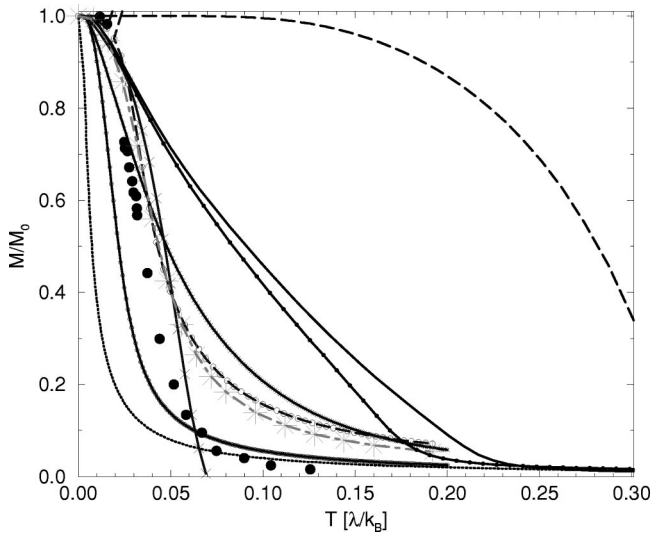

FIG. 9. Results for $M(T)$ at $\Delta_z=0.016\lambda$ for various values of the screening vector k_{sc} and the widths w and α, respectively. The quantity α used in finite-size numerical calculations describes the width of a Gaussian charge distribution in the z direction instead of the width w of a hard-wall quantum well used elsewhere. (1) Free electrons: $w=0$ (dotted curve). (2) SHF: $k_{sc}=0.01l_c^{-1}, w=0$ (long-dashed line). (3) Our theory: $k_{sc}=0.01l_c^{-1}, w=3.11l_c$ (solid line). (4) Our theory: $k_{sc}=0.1l_c^{-1}, w=3.11l_c$ (solid line with dots). (5) Exact diagonalization on the sphere: $N=9, k_{sc}=0, \alpha=0$ (solid line with crosses). (6) Exact diagonalization on the sphere: $N=9, k_{sc}=0, \alpha=2l_c$ (solid line with circles). (7) Sean Barret's experimental data (Ref. 4): $w=3.11l_c$ (filled points). (8) $O(N)$-field theory with $1/N$-corrections (Ref. 7): $w=3.11l_c$ (long dashed line with circles). (9) SU(N)-field theory with $1/N$ corrections (Ref. 7): $w=3.11l_c$ (long dashed line with crosses). (10) Monte Carlo results for the Heisenberg model (Ref. 7): $w=3.11l_c$ (dot-dashed line with stars).

For noninteracting electrons $A_\uparrow(E)=2\pi\delta(E+\Delta_z/2)$ and $M/M_0=\tanh(\beta\Delta_z/4)$. Since interactions tend to favor parallel spin alignment, we expect this result to be a lower bound for M/M_0. As discussed in more detail below, it should become accurate at both high- and low-temperature limits. Note that it reflects the itinerant nature of the electrons which carry the spin magnetization. For localized spin-$\frac{1}{2}$ particles $M/M_0=\tanh(\beta\Delta_z/2)$; the magnetization is smaller at high temperatures in the itinerant case because of the number of many-particle states increases more rapidly with the number of reversed spins. In Hartree-Fock theory, $A_\uparrow(E)=2\pi\delta(E-\xi_\uparrow^{HF})$ and $M/M_0=\tanh[\beta\xi_\downarrow^{HF}(\beta)/2]$. This prediction for the spin magnetization is illustrated in Fig. 9. Because of the exchange-enhanced spin splitting, the magnetization is much larger at fixed temperature than in the noninteracting case. This result grossly overestimates the magnetization because, as in the band theory of metallic magnetism,[32] magnetization suppression due to thermally excited spin waves is not accounted for. These two simple results for M/M_0 should therefore bound the exact result.

Now let us turn to the results obtained using our self-energy approximation, which accounts for electron-spin-wave scattering; numerical results obtained using two different values of k_{sc} are shown in Fig. 9. As explained in Sec. IV, even though the screening wave vector must be finite to ensure convergence of the wave-vector integrals in our self-energy expressions, we do not expect great sensitivity to its value until it becomes comparable to l_c^{-1}. We have estimated the appropriate value for k_{sc} at two different temperatures, as described below. For $T\sim 0.09\lambda/k_B$ and $T\sim 0.18\lambda/k_B$, we find that $k_{sc}=0.01l_c^{-1}$ and $k_{sc}=0.1l_c^{-1}$, respectively. The screening becomes weaker at low temperatures as the system approaches incompressibility. The magnetization curves of Fig. 9 were calculated with these two fixed screening wave vectors; if the screening wave vector were allowed to be temperature dependent, the magnetization value should be above the solid curve in Fig. 9 for temperatures below $0.09\ \lambda/k_B$, should interpolate between the solid curve and the solid curve with dots for temperatures between $0.09\lambda/k_B$ and $0.18\lambda/k_B$, and should be below the solid curve with dots for temperatures beyond $0.18\lambda/k_B$. The comparably weak dependence of the magnetization on the screening wave vector is expected, limiting this source of uncertainty in our predictions. Figure 9 shows that, for $\Delta_z=0.016\lambda$ the magnetization decreases almost linearly with T over a wide range of temperatures between $\sim 0.01\lambda/k_B$ and $\sim 0.2\lambda/k_B$. Over this temperature range, the portion of the spectral weight at $E<0$ is dominated by the low-energy pole, and the Fermi factor evaluated at this pole is still close to 1. Under these conditions the temperature dependence comes nearly entirely from that of the renormalization factor at the low-energy pole, so that $M/M_0\sim(2z-1)\sim 1-(k_BT)\ln(k_BT/\Delta_z)/4\pi\rho_s$. This temperature dependence is identical to what would be obtained from a noninteracting spin-wave model in an external magnetic field $B=\Delta_z/|g\mu_B|$. Ignoring the logarithmic factor, this effect is sufficient to reduce M to small values for $k_BT\sim 4\pi\rho_s\sim 0.3\lambda$, and that is roughly what we observe in Fig. 9.

The accuracy of our calculation of spin-magnetization values is most reliably judged by comparing with results obtained by exact diagonalization of the many-particle Hamiltonian for a small number of electrons on a sphere.[37] In Fig. 9 we present results for the ideal Coulomb interaction obtained for $N=9$ electrons on a sphere, and compare them with the results obtained from our self-energy approximation. We can conclude from this comparison that our self-energy approximation overestimates the magnetization by approximately a factor of 2 at intermediate temperatures. We discuss the physics behind this behavior at greater length below. The magnetization values are least accurate at temperatures between $\sim\Delta_z$ and $\sim 0.1\lambda$ where finite-size effects, discussed below, have some importance and cause the magnetization per particle to be underestimated by finite-size calculations. Nevertheless, it seems clear that our simple self-energy expression results is an overestimate of the magnetization for $0.1\lambda<k_BT<0.3\lambda$. It is interesting to compare these results with essentially exact results for a $S=1/2$ Heisenberg model on a square lattice[7] with a nearest-neighbor exchange interactions whose strength has been adjusted to reproduce the spin stiffness of the quantum Hall ferromagnet. (For the Coulomb model the spin stiffness is known exactly and has the value $\rho_s=\lambda\sqrt{\pi/2}/16\pi$, but is diminished by a factor of 2 due to the finite thickness; see the discussion below.) For the magnetization, this model is accurate when long-length-scale collective magnetization degrees of freedom have dominant importance. The figure shows the results obtained[7] by Timm *et al.* by evaluating

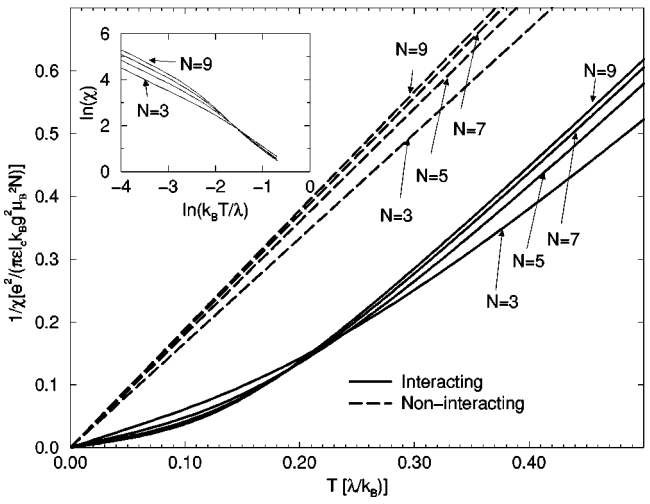

FIG. 10. Numerical finite-size results for the inverse magnetic susceptibility in units of $4\lambda/(g\mu_B)^2N$. In these units the free-electron result is $\chi_0^{-1}=2(k_BT/\lambda)$, and the Hartree-Fock result is $\chi^{-1}=2(k_BT/\lambda-0.3133)$.

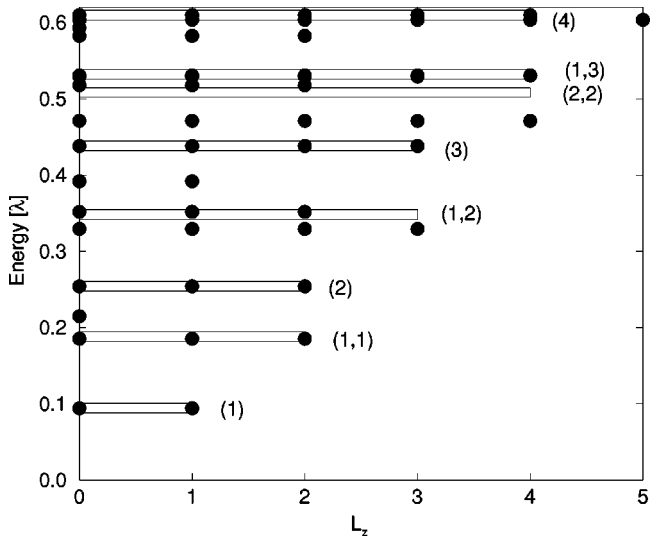

FIG. 11. Low-energy positive L_z excitations for 13 electrons on the surface of a sphere at $\nu=1$. The labels are assignments of linear spin-wave occupations corresponding to the exact eigenstates.

leading $1/N$ corrections to the magnetizations of continuum SU(N) and $O(N)$ models, extending earlier work by Read and Sachdev.[6] At moderate temperatures, the results obtained using these approximation schemes are numerically better than those obtained with our self-energy approximation; they are also somewhat unsatisfactory, however, since the SU(N) scheme leads to negative magnetizations at moderate temperatures and the $O(N)$ scheme fails to capture the low-temperature noninteracting spin-wave limit not shown in the figure. For the temperatures shown the finite width Heisenberg model magnetizations are larger than those of the $N=9$ exact diagonalization calculations, presumably because they have smaller finite-size corrections and are therefore more accurate; see Fig. 9. However, the Heisenberg model $M(T)$ curves for finite width interpolate between the zero width and finite width exact diagonalization data for temperatures between $0.05\lambda<k_BT<0.2\lambda$. The localized spin model $M(T)$ must be above the exact diagonalization results for the electron model at sufficiently high temperatures, where the Heisenberg model magnetization is twice as large as the magnetization of the itinerant-electron system. This is already the case at $k_BT\sim0.2\lambda$ for finite width data. However, the continuum field theory approach cannot address important microscopic electronic properties like the tunneling density of states. We discuss the experimental values of $M(T)$, also shown in this figure, at greater length below.

Our exact diagonalization results for the magnetization have the largest finite-size errors when Δ_z is small. In order to examine the limit of small Δ_z we have calculated the finite-size spin magnetic susceptibility, χ, which is plotted for $N=3$, 5, 7, and 9 in Fig. 10. The noninteracting result, which in the thermodynamic limit approaches $\chi_0=N(g\mu_B)^2/(8k_BT)$, is plotted for comparison. For very high T the Hartree-Fock theory result $\chi^{-1}=8[k_BT-\lambda\tilde{a}(0)/4]/N(g\mu_B)^2$ is approached. However, we see from Fig. 10 that for $T=T_c^{HF}$, where χ diverges in Hartree-Fock theory, it is in fact enhanced by a factor of only ~2.5 compared to the noninteracting electron result. The inset in this figure expands the low-T behavior by plotting $\ln(\chi)$ vs $\ln(k_BT)$. In the thermodynamic limit this quantity should approach[6] $4\pi\rho_s/k_BT$ as $T\to0$. For a finite-size system the low-T limit of χ is the Curie susceptibility associated with the spin-quantum number of the finite-system ground state, $\chi\to(g\mu_B)^2S_0(S_0+1)/3k_BT$, so that $\ln(\chi)$ is a linear function of $\ln(T)$ with an offset which increases with system size. The low-T breaks in the susceptibility plots indicate that finite-size effects become important for temperatures smaller than $\sim0.1\lambda/k_B$, roughly consistent with the temperature below which the microscopic exact diagonalization and Heisenberg model Monte Carlo calculations for zero width differ.

Comparing all these results we can conclude that while our self-energy approximation removes the gross failures of the Hartree-Fock approximation, it still overestimates the spin magnetization at intermediate temperatures. Evidently, interactions between spin waves accelerate the decrease of the magnetization with temperature. We can obtain some corroboration of this interpretation by examining the low-energy portion of the spectrum of the electronic Hamiltonian for $N=13$ shown in Fig. 11. These results are for electrons on the surface of a sphere. All excited states with positive total L_z are shown. The largest value of L_z for which a state occurs specifies its total angular momentum. The various eigenenergies are labeled by the occupation numbers of the corresponding noninteracting spin-wave states. Where the occupation number exceeds 1, the label of the spin-wave state is repeated so that the number of labels is equal to the total spin-wave occupation number of the state. Single-spin-wave states occur in the $S=N/2-1$ portion of the spectrum. The lowest-energy multiple spin-wave state is the (1,1) state, where the $L=1$ spin wave is doubly occupied. Since there are three degenerate spin waves with $L=1$, if there were no spin-wave interactions, the six (1,1) two bosons states would be degenerate and would have an energy equal to twice the energy of the $L=1$ single-spin-wave state. The open horizontal bars in Fig. 11 indicate the noninteracting spin-wave energies. We see there that spin-wave interactions split the six (1,1) states into a fivefold-degenerate $L=2$ level and a

single $L=0$ level. Generally, multiple-spin-wave states are reduced in energy by interactions, and this effect leads to a magnetization which decreases more rapidly with increasing temperature than would be expected if spin-wave interactions were neglected. This is most apparent in Fig. 11 in the effect of interactions on the energies of the 15 expected (2,2) two-boson states. When interactions are included these states are split into $L=4$, 2, and 0 levels. We see in Fig. 11 that the $L=4$ level, which has the largest degeneracy, is lowered in energy by spin-wave interactions.

We now turn to a comparison between theory and experiment.[4,5] An important source of uncertainty is introduced by the dependence of the effective interaction between 2D electrons[39] on the width, as already mentioned, and, to a lesser degree, the height of the quantum well containing the electrons. For a quantum well of width w and infinite barrier heights, the effective interaction[28] is $\tilde{V}_{eff}(\vec{k})=F(\vec{k})\tilde{V}(\vec{k})$, where[38]

$$F(k,w)=\frac{32\pi^4(e^{-kw}-1)}{[kw(4\pi^2+k^2w^2)]^2}+\frac{8\pi^2}{[kw(4\pi^2+k^2w^2)]}+\frac{3kw}{(4\pi^2+k^2w^2)}. \tag{45}$$

When the system is described by phenomenological field theory or Heisenberg models, the microscopic physics enters only through the spin stiffness. The analytic expression relating spin stiffness ρ_s and quantum-well width w for the case of a quantum well with infinite barrier heights via the effective interaction $\tilde{V}_{eff}(\vec{k})$ (Ref. 15) at $\nu=1$ is

$$\rho_s=\frac{\lambda l_c^2}{32\pi^2}\int_0^\infty dk k^3\tilde{V}_{eff}(k)\exp(-k^2l_c^2/2). \tag{46}$$

The k^3 factor in this integrand is responsible for considerable sensitivity of ρ_s to $\tilde{V}_{eff}(k)$ at large k, where the finite thickness corrections appear. For comparison the spin-splitting gap $\tilde{a}(0)$ has a considerably weaker relative dependence on the well width. The spin stiffness is reduced by approximately a factor of 2 compared to the zero-width 2D layer case for quantum wells with a width $w=3l_c$. This is actually close to the typical experimental situation where the quantum well widths are $\sim$30 nm and the fields are $\sim$10 T. We remark that this reduction of ρ_s reduces the temperature interval over which collective excitations are dominant and the field-theory and Heisenberg phenomenological models are appropriate. In Fig. 9 we compare experimental data with exact diagonalization calculations of the spin magnetization which account for finite-well thickness. For the purpose of this comparison, we consider the exact diagonalization results to be essentially exact for a model which neglects disorder and Landau-level mixing. Compared to the best fits, the experimental magnetization decreases too slowly at low temperatures, and too quickly at high temperatures. It seems clear that the experimental values are too low at the highest temperatures, where they fall below even the noninteracting system magnetizations (this happens for $k_BT\sim0.09$ in Barrett's experiment). The weaker T dependence at low T in the experimental data could be due to disorder, and in particular to weak large length-scale inhomogenity, which is neglected in all theoretical models discussed here.

Finally, we comment on the role of skyrmions. One of the interesting results of the NMR experiments was the experimental evidence for skyrmions at filling factors near 1.[4] Our diagrammatic theory is not able to account for skyrmions, although we know that neutral Skyrmion–anti-Skyrmion pair excitations exist at $\nu=1$. Their total energy for $\Delta_z=0$ is only half of that of the quasielectron-quasihole pair, although the energetic advantage drops quickly with increasing Zeeman gap (see Fig. 1 in Ref. 40). Thus the existence of such excitations at the upper end of the excitation spectrum should not dramatically alter the thermodynamics.

B. Nuclear-spin-relaxation rate

The optically pumped NMR experiments of Barrett *et al.* can also be used to measure the rate of nuclear-spin-relaxation due to coupling to the electronic spins. At present, measurements of the temperature dependence of the relaxation time over a broad range of temperatures at $\nu=1$ are unavailable. The Korringa theory of nuclear-spin relaxation in a metal[41] can be generalized to electrons in a quantum well with the result[42]

$$T_1^{-1}=\frac{k_BTA^2\Omega^2|\phi(z)|^4}{(g\mu_B)^2\hbar}\lim_{\omega\to0}\frac{\mathrm{Im}\,\chi^{+-}(\vec{r},\vec{r};\omega)}{\hbar\omega}. \tag{47}$$

In this equation A is the hyperfine coupling constant, Ω is the unit-cell volume, and $\phi(z)$ is the envelope function of the electronic quantum-well state. The influence of interactions on the relaxation rate was studied in the limit where disorder is relatively strong and interactions can be treated perturbatively.[43,30] If we neglect vertex corrections, the local response function χ^{+-} in Eq. (47) can be expressed in terms of the spectral function for the one-particle Green's function. The result for the relaxation rate of nuclei at the center of the quantum well is

$$T_1^{-1}=C(B,w)\frac{k_BT}{\lambda}\int_{-\infty}^{\infty}\frac{dE}{(2\pi)^2}\frac{-\partial n_F(E)}{\partial E}\lambda^2A_\uparrow(E)A_\downarrow(E). \tag{48}$$

Inserting GaAs parameters[42] for the prefactor in Eq. (48) gives $C(B,w)=0.47(B[\mathrm{T}])^{3/2}/(w[\mathrm{nm}])^2$ Hz. For typical fields and quantum-well widths the prefactor corresponds to a relaxation time $\sim$100 s. The dimensionless integral in Eq. (48), which gives the relaxation rate in this unit, is plotted as a function of temperature in Fig. 12. Existing experimental data cover only the low-temperature limit, and are consistent with the very long relaxation times indicated here. Contributions to the relaxation rate come dominantly from the continuum portion of the spectral weight near zero energy. In our theory this is small at both low and high temperatures. Since T_1^{-1} measures the low-energy spin-flip excitations of the system, it is amenable to an analysis based on the continuum field theory model, which has also been used to obtain theoretical estimates of its temperature dependence.[6] It should, in principle, be possible to extract more information about the spectral functions, including information on its behavior far from the Fermi energy where a microscopic theory

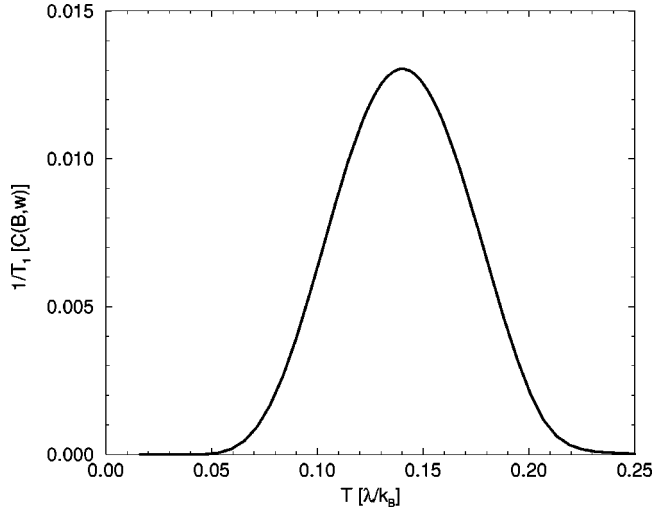

FIG. 12. Nuclear-spin-relaxation rate as a function of temperature in units of the field- and quantum-well-width-dependent prefactor $C(B,w)$ discussed in the text. The prefactor becomes 9.8×10^{-3} Hz for a magnetic field $B=7.05T$ and $w=3.11l_c(k_{sc}=0.01l_c^{-1})$.

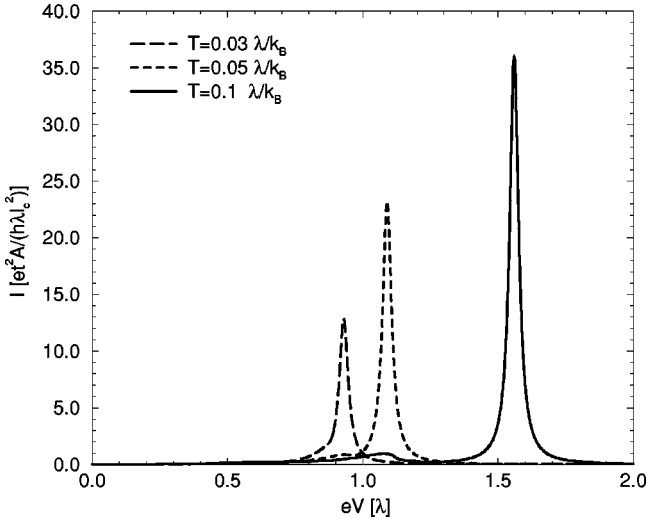

FIG. 13. Tunneling current-voltage relation as a function of bias voltage at $\nu=1$ for three temperatures $T=0.03$, 0.05, and $0.1\lambda/k_B$, where the δ peaks of the spectral functions are replaced by Lorentzians with width $\epsilon=0.01\lambda$. The parameters used for this calculation are: $\Delta_z=0.016\lambda$, $w=3.11l_c$, and $k_{sc}=0.01l_c^{-1}$.

is necessary, from the 2D-2D tunneling studies of quantum Hall ferromagnets, which we propose below.

C. Tunneling current

Electronic spectral functions are traditionally measured by tunneling experiments. The measurement[44] of spectral functions for 2D electron systems is enabled by techniques[45] for making separate contact between nearby quantum wells. In the absence of a magnetic field, this technique has made it possible to measure the quasiparticle lifetime including its dependence on temperature due to carrier-carrier scattering. For strong magnetic fields[46,47] the tunneling current is related to the bias voltage by

$$I(V)=\frac{et^2A}{h\lambda l_c^2}\int_{-\infty}^{\infty}\frac{dE}{2\pi}[n_F(E-eV)-n_F(E)]\lambda \times\sum_{\sigma} A_\sigma(E)A_\sigma(E-eV). \tag{49}$$

Here t is the tunneling amplitude and A the area of the 2D system. We caution that the above formula applies when both 2D layers are kept at filling factor $\nu=1$ in the presence of a bias voltage. In 2D-2D tunneling, layer densities change with bias potential because of the finite capacitance of the double-layer system, unless a compensating gate voltage is applied. This issue is especially important at $\nu=1$ because of the sensitivity of the electron system to density near this filling factor. Provided that there is no density change in either layer, each spin direction contributes equally to the current. Measurements at fractional filling factors have demonstrated a deep, wide, and only partially understood minima in the spectral function near zero energy. Our calculations suggest the possibility of further interesting findings when experiments are performed at $\nu=1$. In Fig. 13 we plot the dependence of the tunneling current on bias voltage for three temperatures. Within our theory a δ peak with a substantial weight proportional to $zz^+\sim[1-(M/M_0)^2]/4$ appears. This peak arises from the product of the two poles in the spectral function, and it will occur at a temperature dependent value of eV equal, for the idealized case of a zero-width quantum well, at the energy difference between the upper and lower pole positions plotted in Fig. 8. Broader and much weaker features result from the convolution of a δ-function peak with the continuum contribution, and still broader and weaker features from the self-convolution of the continuum contributions to the spectral functions. Only this last contribution contributes to the linear tunneling conductance. In Fig. 13 we have for visualization purposes arbitrarily replaced the δ-function contribution by a Lorentzian of width 0.01λ.

We expect that sharp peaks do occur at voltages near the exchange splitting, despite the quantitative limitations of our theory discussed above. In Fig. 14 we plot the tunneling conductance

$$G=\lim_{V\to 0}\frac{I}{V}=\frac{e^2}{h}\frac{t^2A}{\lambda^2 l_c^2}\int_{-\infty}^{\infty}\frac{dE}{2\pi}\frac{-\partial n_F(E)}{\partial E}\lambda^2\sum_{\sigma} A_\sigma(E)^2 \tag{50}$$

as a function of temperature. The tunneling conductance is proportional to the square of the spectral function averaged over energy arguments less than $\sim k_BT$. It therefore has a temperature dependence similar to that of the nuclear-spin relaxation rate. It vanishes at zero temperature and remains small even for k_BT substantially in excess of Δ_z since the bulk of the spectral weight is shared between the high- and low-energy poles and exchange-enhanced spin splitting causes these to be well away from the chemical potential.

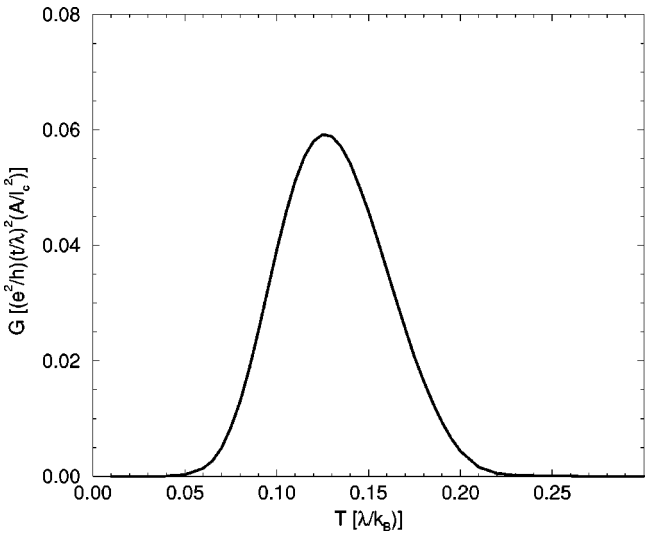

FIG. 14. Tunneling conductance in the limit of vanishing voltage as a function of temperature at $\nu=1$ for the quantum-well width $w=3.11l_c$ and $\Delta_z=0.016\lambda$ ($k_{sc}=0.01l_c^{-1}$).

VI. ODDS AND ENDS

A. Consistency

A second formally exact expression can be derived which relates the electronic spectral function to the magnetization. In the strong-field limit, $K=H-\mu N=K_\uparrow+K_\downarrow$ can[24] be written as

$$K_\sigma(T,V,\mu)=\frac{N_\Phi}{2\beta}\sum_{i\nu_n} e^{i\nu_n\eta}[i\hbar\nu_n+\xi_\sigma^{(0)}]\mathcal{G}_\sigma(i\nu_n), \quad (51)$$

where η is a positive infinitesimal and the sum is over Matsubara frequencies. Using the spectral representation of the Matsubara Green's function and performing a contour integral then yields

$$K_\sigma(T,V,\mu)=\frac{N_\Phi}{2}\int_{-\infty}^{\infty}\frac{dE}{2\pi}n_F(E)(E+\xi_\sigma^{(0)})A_\sigma(E). \quad (52)$$

Using thermodynamic identities, the magnetization can in turn be expressed in terms of K:

$$M(T,V,\mu)=-\frac{1}{\beta}\int_0^\beta d\beta'\left(\frac{\partial K}{\partial B}\right)_{\beta',V,\mu}. \quad (53)$$

We do not obtain the same result for M from this expression as from the more direct expression discussed above if we go beyond the SHF approximation. This ambiguity is one of several consequences of the fact that our self-energy approximation is defined in terms of Hartree-Fock propagators, and is not conserving.[48]

Some partial self-consistency can be achieved by simply replacing the SHF occupation factors ξ_σ^{HF}, wherever they appear, by occupation factors calculated from the final spectral functions. At $\nu=1$, it is sufficient to specify the difference of majority- and minority-spin filling factors $\Delta\nu$. Following this procedure requires that we solve an equation of the form $\Delta\nu=f(\Delta\nu)$, where f incorporates the entire functional dependence on the right-hand side of Eq. (44). At the same time, we modify the HF quasiparticle energy accordingly:

$$\xi_\uparrow=-\frac{1}{2}[\Delta_z+\lambda\tilde{a}(0)\Delta\nu]. \quad (54)$$

Together with Eq. (44) this procedure defines an implicit equation for the difference $\Delta\nu$, i.e., for the magnetization. In general this equation has at least one solution with $0<\Delta\nu<\Delta\nu^{HF}$. We have determined this solution as a function of temperatures and have found that the solution is unique. The result was shown in Fig. 3 in Ref. 9. The smaller magnetization values are in better accord with experiment. The improvement probably does reflect a partial accounting of omissions of the elementary electron spin-wave scattering theory. However, the abrupt decrease of the magnetization toward noninteracting electron values at temperature values $T\sim 0.06\lambda/k_B$ is certainly unphysical. Not surprisingly, this *ad hoc* procedure does not provide satisfying results. A more elaborate attempt at a self-consistent scheme, in which the full set of equations (28) was solved self-consistently, has been explored by Haussmann,[10] and proved to be equally unsatisfying.

Some hints at possible routes toward a more accurate theory can be found in examinations of the transverse susceptibility of a quantum Hall ferromagnet. It is remarkable[16] that in the LLL, this quantity can be expressed exactly as a geometric series of of irreducible particle-hole bubbles $[\bar{\Phi}(\vec{q},i\omega_n)]$,

$$\bar{\chi}^{+-}(\vec{q},i\omega_n)=\frac{\bar{\Phi}(\vec{q},i\omega_n)}{1+I(\vec{q})\bar{\Phi}(\vec{q},i\omega_n)}, \quad (55)$$

where $I(\vec{q})$ is independent of frequency. In the generalized random-phase approximation, $\bar{\Phi}(\vec{q},i\omega_n)$ is approximated by a bubble with Hartree-Fock propagators. Generally, the irreducible particle-hole bubble can be expressed in terms of an irreducible vertex function $\bar{\gamma}[\vec{q};i\nu_n\uparrow;i(\nu_n+\omega_n),\downarrow]$:

$$\bar{\Phi}(\vec{q},i\omega_n)=-(g\mu_B)^2\frac{e^{-q^2l_c^2/2}}{2\pi l_c^2}\times\frac{1}{\beta}\sum_{i\nu_n}\bar{\gamma}[\vec{q};i\nu_n\uparrow;i(\nu_n+\omega_n)\downarrow]\times\mathcal{G}_\uparrow(i\nu_n)\mathcal{G}_\downarrow[i(\nu_n+\omega_n)]. \quad (56)$$

In the RPA expression for $\bar{\Phi}$ we have set $\bar{\gamma}=1$, and the GF's are approximated by the SHF GF's. Therefore it is not surprising that any improvement of $\mathcal{G}$ beyond the SHF GF makes a change of $\bar{\gamma}$ necessary in order to satisfy the Goldstone theorem condition $1=-I(\vec{0})\bar{\Phi}(0,0)$.

B. Screening

In any electronic system, screening of electron-electron interactions plays an important role in many-particle physics.

The simplest approximation for the dynamically screened interaction is the RPA, which, for the present problem, takes the form

$$\tilde{V}(\vec{k},i\omega_n)=\frac{\tilde{V}_c(\vec{k})}{\epsilon(\vec{k},i\omega_n)}=\frac{\tilde{V}_c(\vec{k})}{1+\tilde{V}_c(\vec{k})\Pi^0(\vec{k},i\omega_n)}=\frac{2\pi l_c}{k+2\pi l_c\Pi^0(\vec{k},i\omega_n)}, \tag{57}$$

with the polarization function approximated by

$$\Pi^0(\vec{k},i\omega_n)=-\frac{e^{-k^2l_c^2/2}}{2\pi l_c^2}\frac{\lambda}{\beta}\sum_{i\nu_n,\sigma}\mathcal{G}_\sigma^{HF}(i\nu_n)\mathcal{G}_\sigma^{HF}[i(\nu_n-\omega_n)]. \tag{58}$$

In this approximation, Landau-level degeneracy is responsible for polarization functions, which vanish at nonzero Matsubara frequencies. At $i\omega_n=0$, we find that

$$\tilde{V}(\vec{k},i\omega_n=0)=\frac{\tilde{V}_c(\vec{k})}{1+\tilde{V}_c(\vec{k})\beta\lambda\dfrac{e^{-k^2l_c^2/2}}{2\pi l_c^2}\displaystyle\sum_\sigma n_F(\xi_\sigma^{HF})[1-n_F(\xi_\sigma^{HF})]}. \tag{59}$$

In the long-wavelength limit this leads to the following expression for the temperature-dependent screening wave vector at $\nu=1$:

$$k_{sc}(T)=\frac{2\beta\lambda}{l_c}n_F(\xi_\uparrow^{HF})[1-n_F(\xi_\uparrow^{HF})]=\frac{\beta\lambda}{2l_c\cosh^2[\beta\xi_\uparrow^{HF}(k_{sc},\beta)/2]}. \tag{60}$$

The inclusion of interaction effects in the HF energies plays an important role in the temperature dependence of k_{sc} implied by this equation. At low temperatures the screening wave vector $k_{sc}\sim\exp(-\xi_\downarrow^{HF}/k_BT)/k_BT$ is extremely small. The limited utility of this screening approximation is evidenced by the discontinuous dependence of k_{sc} on temperature found when Eq. (60) is solved numerically.

Additional insight into screening in the static long-wavelength limit can be obtained by using Thomas-Fermi theory, in which

$$k_{sc}(T)=2\pi l_c\lambda n^2\kappa=2\pi l_c\lambda\left(\frac{\partial n}{\partial\mu}\right)_{T,V,N}=\frac{\lambda}{l_c}\left(\frac{d\nu}{d\mu}\right)_{T,V,N}, \tag{61}$$

where κ is the compressibility, n is the particle density, and $\nu=2\pi l_c^2n$. If we neglect the dependence of the spectral function on the chemical potential μ and exploit particle-hole symmetry at $\nu=1$, we obtain

$$k_{sc}=\frac{2\beta\lambda}{l_c}\int_{-\infty}^{\infty}\frac{dE}{(2\pi)}A_\uparrow(E)n_F(E)[1-n_F(E)]. \tag{62}$$

This is an implicit equation for k_{sc}, since $A_\uparrow(E)$ itself depends on $\xi_\uparrow^{HF}$, which again depends on $\tilde{a}(0)$ and thus on k_{sc} [see Eq. (6)]. With this equation we can use the improved spectral density of the spin-wave theory to estimate the approximate magnitude of wave vector k_{sc} at a given temperature. Rather than solving self-consistently for k_{sc} at each temperature, we have fixed k_{sc} at two values, and used Eq. (62) to find those temperatures at which these values are self-consistent. As discussed in Sec. V, this procedure is adequate given the relatively weak sensitivity of our results at low and moderate temperatures to the value used for k_{sc}. At higher temperatures, screening is likely to be important since stronger screening causes a flattening of the spin-wave dispersion, which leads in turn to more magnetization suppression, smaller exchange splittings, more mobile charges, and hence still stronger screening.

C. High-temperature behavior

The high-temperature expansion of the magnetization gives us some insight into the validity of our approximations and stresses the importance of screening at higher temperatures. However, these results are of rather theoretical interest because at large temperatures excitations to higher orbital Landau levels become more and more probable and our restriction to the LLL becomes questionable.

In principle, the many-body perturbation theory expansion for the thermodynamic potential provides a systematic order by order expansion in powers of the interaction strength over the bare Zeeman gap, or the temperature or combinations thereof. However, the long range of the Coulomb interaction gives rise to divergent diagrams and complicates issues again; for example, a logarithmically divergent contribution to the magnetization appears at third order in interaction strength, which can be traced back to the divergent second-order bubble diagram for the self-energy. A systematic way to circumvent this problem is to expand in terms of interactions, which are screened by infinite-order bubble diagram partial summations. Rather than pursuing this line, we have attempted to gain some insight from perturbative expansions by performing the expansion up to third order in β for the case of hard-core interaction model with $\tilde{V}(q)=4\pi V_0l_c^2$.[49]

The leading term of the high-temperature expansion for the spin magnetization is identical to the same term for free particles, i.e., the lowest order term in the expansion of $M(T)/M_0=\tanh(\beta\Delta_z/4)=\beta\Delta_z/4+O(\beta^2)$. As mentioned previously, this limit shows that the Heisenberg model, which yields a magnetization that is twice of this value, fails once itinerancy becomes important. Our calculations are based on the linked-cluster coupling-constant-integration expansion of the thermodynamic potential.[50] The leading correction, which is quadratic in β, is determined solely by the exchange integral $2V_0$ and leads to an increase of the spin magnetization. We have carried this expansion out to third order, and find that

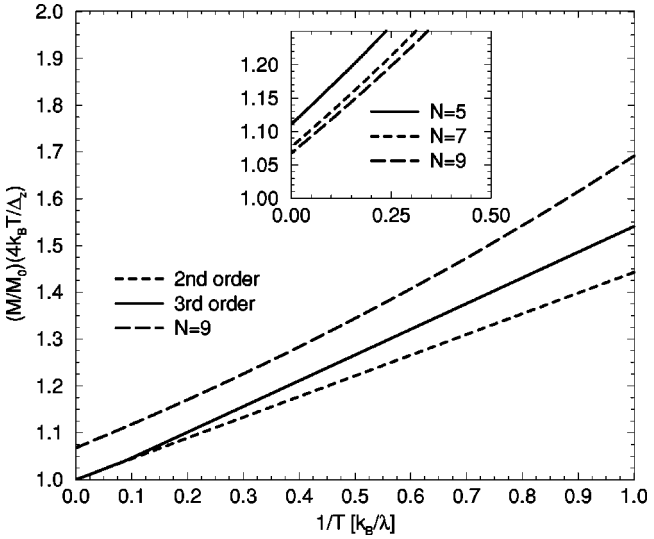

FIG. 15. Spin magnetization to third order in $1/T$ normalized by the high-temperature free-particle magnetization $[\Delta_z/(4k_BT)]$ for the hard-core model ($V_0=\sqrt{\pi}/2$, $\Delta_z=0.016\lambda$, and $w=0.0$). The resulting deviation of the nine-particle exact diagonalization is due to finite-size effects whose diminishing influence with increasing particle number is shown in the inset.

$$M=M_0\frac{\beta\Delta_z}{4}\left\{1+\frac{\beta V_0\lambda}{2}+\frac{\beta^2}{8}\left(V_0^2\lambda^2-\frac{\Delta_z^2}{6}\right)\right\}+O(\beta^4). \tag{63}$$

Note that the V_0^2 term also contributes positively to the magnetization. Figure 15 shows MT/M_0 vs $1/T$ at high temperatures. We can see from this figure that beyond leading-order interaction contributions become important for k_BT smaller than $\approx 2.5\lambda$. For comparison the results from exact diagonalizations for fixed particle numbers are given, which show the right slope but exhibit finite-size corrections of the expected order of magnitude.[51] Obviously the importance of correlations in this system persists to high temperatures. This property is a key in validating the use of models, which correctly describe only collective fluctuations in magnetization, even when k_BT is not small compared to underlying interaction energy scales.

VII. SUMMARY AND CONCLUSIONS

In this paper we report on a study of the one-particle Green's function of a quantum Hall system at filling factor $\nu=1$. The ground state of the two-dimensional electron system in this case is a strong ferromagnet. Many analogies exist between the properties and the theoretical description of this system and conventional metallic ferromagnets. At $\nu=1$ the ground state and the elementary excitations of quantum Hall ferromagnets are given exactly by time-dependent Hartree-Fock theory. This success is analogous to the success of band theory in describing the ground state and both collective and particle-hole elementary excitations of band ferromagnets. At finite temperatures, however, we show that Hartree-Fock theory fails qualitatively for quantum Hall ferromagnets, just as band theory fails for metallic ferromagnets. Our work is based on an improved approximation for the electron self-energy, which describes the scattering of fermionic quasiparticles off the spin-wave collective excitations composed of coherent combinations of spin-flip particle-hole excitations. This perturbative approximation is equivalent to ones which have been used[33] for models of itinerant-electron ferromagnets at finite temperatures. Here we have the advantage that complicated band structures do not confuse a comparison of theory and experiment. We find that, at intermediate temperatures where the density of spin-wave excitations is high, although our approximation gives a huge improvement over Hartree-Fock theory, it still overestimates the magnetization by nearly a factor of 2. We attribute this failure to the neglect of interactions between spin waves in our approximation. Nevertheless, we expect that the qualitative physics predicted by our approximation is correct. On the basis of our calculations we predict that a sharp peak will occur in 2D-2D tunneling current when the bias energy eV is approximately equal to the spin splitting, and that the strength of this peak will be approximately proportional to temperature at low T. This peak is due to fluctuations in the direction of the exchange field, which separates the energy of majority- and minority-spin quasiparticles. We have recently argued[36] that in metallic ferromagnets, this mechanism is responsible for the temperature dependence of magnetoresistance in ferromagnetic tunnel junctions. In that case, however, the mechanism cannot be directly verified by tunneling experiments because the width of the quasiparticle bands is comparable to their exchange spin splitting. Verification of the predicted effect in quantum Hall ferromagnets, therefore, has important implications for metallic magnetic tunnel junctions.

ACKNOWLEDGMENTS

We thank S. Barrett for sharing data from the NMR measurements of his group prior to publication, and to P. Henelius and C. Timm for providing data on the Heisenberg model calculation. Discussions with W. Apel, S. M. Girvin, B. Goldberg, C. Hanna, R. Haussmann, H. Mori, and S. Sachdev are gratefully acknowledged. One of the authors (M. K.) was supported by the German Academic Exchange Service (DAAD). This work was supported in part by NSF Grant No. DMR97-14055. J.J.P. acknowledges support by NSF Grant No. DMR95-03814 and by the MEC of Spain under Contract No. PB96-0085.

[1] A. H. MacDonald, H. A. Fertig, and L. Brey, Phys. Rev. Lett. **76**, 2153 (1996).

[2] For a review of quantum Hall ferromagnets, see S. M. Girvin and A. H. MacDonald, in *Novel Quantum Liquids in Low-Dimensional Semiconductor Structures*, edited by S. Das Sarma and A. Pinczuk (Wiley, New York, 1996). For a brief and elementary discussion, see A. H. MacDonald, Solid State Commun. **102**, 143 (1997).

[3] For reviews of theoretical work on itinerant-electron ferromagnets, see C. Herring, in *Magnetism*, edited by G. T. Rado and H.

Suhl (Academic, New York, 1966), Vol. 4, and T. Moriya, *Spin Fluctuations in Itinerant Electron Magnetism*, Solid State Science Vol. 56 (Springer-Verlag, Berlin, 1985).

[4] S. E. Barrett, G. Dabbagh, L. N. Pfeiffer, K. W. West, and R. Tycko, Phys. Rev. Lett. **74**, 5112 (1995).

[5] M. J. Manfra, E. H. Aifer, B. B. Goldberg, D. A. Broido, L. Pfeiffer, and K. West, Phys. Rev. B **54**, R17 327 (1996).

[6] N. Read and S. Sachdev, Phys. Rev. Lett. **75**, 3509 (1995).

[7] C. Timm, S. M. Girvin, P. Henelius, and A. W. Sandvik, Phys. Rev. B **58**, 1464 (1998).

[8] As we see below, however, the present work suggests that in the case of long-range electron-electron interactions the spin-stiffness energy may *not* completely determine the low-temperature, weak Zeeman coupling physics.

[9] Marcus Kasner and A. H. MacDonald, Phys. Rev. Lett. **76**, 3204 (1996).

[10] R. Haussmann, Phys. Rev. B **53**, 7357 (1996); **56**, 9684 (1997).

[11] R. O. Jones and O. Gunnarson, Rev. Mod. Phys. **61**, 689 (1989).

[12] See, for example, A. H. MacDonald, Phys. Rev. B **30**, 4392 (1984).

[13] The undependable nature of conclusions based on pure Hartree-Fock or Hund's rule arguments is emphasized by their failure away from $\nu=1$.

[14] This simple result for $\nu=1$ cannot immediately be generalized to other QHE filling factors. For example, at filling factor $\nu=2/3$ the ground state appears to be a spin singlet for $g=0$. See, for example, T. Chakraborty and P. Pietiäinen, Phys. Rev. Lett. **76**, 4018 (1996), and work cited therein.

[15] Kun Yang, K. Moon, L. Zheng, A. H. MacDonald, S. M. Girvin, D. Yoshioka, and S.-C. Zhang, Phys. Rev. Lett. **72**, 732 (1994); K. Moon, H. Mori, Kun Yang, S. M. Girvin, A. H. MacDonald, L. Zheng, D. Yoshioka, and S.-C. Zhang, Phys. Rev. B **51**, 5138 (1995).

[16] M. Kasner (unpublished).

[17] Yu. A. Bychkov, S. V. Iordanskii, and G. M. Eliashberg, Pis'ma Zh. Éksp. Teor. Fiz. **33**, 152 (1981) [JETP Lett. **33**, 143 (1981)].

[18] C. Kallin and B. I. Halperin, Phys. Rev. B **30**, 5655 (1984).

[19] M. Rasolt and A. H. MacDonald, Phys. Rev. B **34**, 5530 (1986); A. H. MacDonald and G. C. Aers, *ibid.* **34**, 2906 (1986).

[20] A. H. MacDonald, J. Phys. C **18**, 1003 (1985).

[21] In the case of no screening $k_{sc}=0$, we recover the well-known explicit expression $\tilde{a}(k)=\sqrt{\pi/2}e^{-k^2l_c^2/4}I_0(k^2l_c^2/4)$.

[22] See, for example, A. H. MacDonald, in *Proceedings of the Les Houches Summer School on Mesoscopic Physics*, edited by E. Akkermans, G. Montambeaux, J.-L. Pichard, and J. Zinn-Justin (North-Holland, Amsterdam, 1995).

[23] S. L. Sondhi, A. Karlhede, S. A. Kivelson, and E. H. Rezayi, Phys. Rev. B **47**, 16 419 (1993); H. A. Fertig, L. Brey, R. Cote, and A. H. MacDonald, *ibid.* **50**, 11 018 (1994); A. H. MacDonald, H. A. Fertig, and L. Brey, Phys. Rev. Lett. **76**, 2153 (1996); H. A. Fertig, Luis Brey, R. Côté, A. H. MacDonald, A. Karlhede, and S. L. Sondhi, Phys. Rev. B **55**, 10 671 (1997); M. Abolfath, J. J. Palacios, H. A. Fertig, S. M. Girvin, and A. H. MacDonald, *ibid.* **56**, 6795 (1997).

[24] A. L. Fetter and J. D. Walecka, *Quantum Theory of Many-Particle Systems* (McGraw-Hill, New York, 1971), p. 261.

[25] John W. Negele and Henri Orland, *Quantum Many-Particle Systems* (Addison-Wesley, New York, 1988).

[26] G. D. Mahan, *Many-Particle Physics* (Plenum Press, New York, 1990), p. 176.

[27] A. H. MacDonald and S. M. Girvin, Phys. Rev. B **38**, 6295 (1988).

[28] T. Ando and Y. Uemura, J. Phys. Soc. Jpn. **37**, 1044 (1974).

[29] A. Usher, R. J. Nicholas, J. J. Harris, and C. T. Foxon, Phys. Rev. B **41**, 1129 (1990).

[30] D. Antoniou and A. H. MacDonald, Phys. Rev. B **43**, 11 686 (1991). This paper examines the influence of disorder on the dynamic susceptibility.

[31] E. C. Stoner, Philos. Mag. **17**, 1018 (1933); J. C. Slater, Phys. Rev. **49**, 537 (1936).

[32] See, for example, A. T. Alfred, Phys. Rev. B **11**, 2597 (1975); G. Lonzarich and A. V. Gold, Can. J. Phys. **52**, 694 (1974); D. M. Edwards, *ibid.* **52**, 704 (1974); V. Korenman, J. L. Murray, and R. E. Prange, Phys. Rev. B **16**, 4032 (1977), and work cited therein.

[33] J. A. Hertz and D. M. Edwards, J. Phys. F: Met. Phys. **3**, 2174 (1973), **3**, 2191 (1973).

[34] The influence of dynamic screening on exchange-enhanced spin-splitting of Landau levels at moderate field strengths was studied by A. P. Smith, A. H. MacDonald, and G. Gumbs, Phys. Rev. B **45**, 8829 (1992).

[35] Kun Yang and A. H. MacDonald, Phys. Rev. B **51**, 17 247 (1995).

[36] Spectral function evolution with temperature does, however, play a role in the junction magnetoresistance of magnetic tunnel junctions: A. H. MacDonald, T. Jungwirth, and M. Kasner, Phys. Rev. Lett. **81**, 705 (1998).

[37] Similar results were reported by T. Chakraborty and P. Pietiläinen, Phys. Rev. Lett. **76**, 4018 (1996); T. Chakraborty, P. Pietiläinen, and R. Shankar, Europhys. Lett. **38**, 141 (1997).

[38] The given form factor $F(k,w)$ is based on a symmetric charge distribution $\rho(z)\sim\sin^2(\pi z/w)$ for the electrons in a quantum well of width w. See R. Tycko, S. E. Barrett, G. Dabbagh, L. N. Pfeiffer, and K. W. West, Science **268**, 1460 (1995).

[39] See, for example, T. Ando, A. B. Fowler, and F. Stern, Rev. Mod. Phys. **54**, 437 (1982); A. H. MacDonald and G. C. Aers, Phys. Rev. B **29**, 5976 (1984).

[40] H. A. Fertig, L. Brey, R. Côté, and A. H. MacDonald, Phys. Rev. B **50**, 11 018 (1994).

[41] C. P. Slichter, *Principles of Magnetic Resonance* (Springer-Verlag, Berlin, 1990).

[42] A. Berg, M. Dobers, R. R. Gerhardts, and K. v. Klitzing, Phys. Rev. Lett. **64**, 2563 (1990).

[43] I. D. Vagner and T. Maniv, Phys. Rev. Lett. **61**, 1400 (1988); T. Maniv and I. D. Vagner, Surf. Sci. **229**, 134 (1990).

[44] L. Zheng and A. H. MacDonald, Phys. Rev. B **47**, 10 619 (1993); T. Jungwirth and A. H. MacDonald, *ibid.* **53**, 7403 (1996); L. Zheng and S. DasSarma, *ibid.* **53**, 9964 (1996).

[45] J. P. Eisenstein, L. N. Pfeiffer, and K. W. West, Appl. Phys. Lett. **58**, 1497 (1991); J. Smoliner, E. Gornik, and G. Weimann, *ibid.* **52**, 2136 (1988); J. P. Eisenstein, T. J. Gramila, L. N. Pfeiffer, and K. W. West, Phys. Rev. B **44**, 6511 (1991); R. C. Ashoori and R. H. Silsbee, Solid State Commun. **81**, 821 (1992); S. Q. Murphy, J. P. Eisenstein, L. N. Pfeiffer, and K. W. West, Phys. Rev. B **52**, 14 825 (1995).

[46] P. Johansson and J. M. Kinaret, Phys. Rev. Lett. **71**, 1435 (1993); A. L. Efros and F. G. Pikus, Phys. Rev. B **48**, 14 694 (1993); C. M. Varma, A. I. Larkin, and E. Abrahams, *ibid.* **49**, 13 999 (1994); I. L. Aleiner, H. U. Baranger, and L. I. Glazman, Phys. Rev. Lett. **74**, 3435 (1995); Rudolf Haussmann, Hiroyuki Mori, and A. H. MacDonald, *ibid.* **76**, 979 (1996).

[47] J. P. Eisenstein, L. N. Pfeiffer, and K. W. West, Phys. Rev. Lett. **74**, 1419 (1995); R. C. Ashoori, J. A. Lebens, N. P. Bigelow, and R. H. Silsbee, Phys. Rev. B **48**, 4616 (1993); K. M. Brown, N. Turner, J. T. Nicholls, E. H. Linfield, M. Pepper, D. A. Ritchie, and G. A. C. Jones, *ibid.* **50**, 15 465 (1994).

[48] G. Baym, Phys. Rev. **127**, 1391 (1962); G. Baym and L. P. Kadanoff, *ibid.* **124**, 287 (1961).

[49] For the numerical evaluation of our expressions we choose the value $V_0=\sqrt{\pi}/2$, which equals the zero momentum pseudopotential in the expansion of the Coulomb interaction in the LLL. In contrast to the Coulomb model there is no neutralizing background in the hard core interaction model. Therefore, tadpole diagrams have to be considered.

[50] M. Kasner, Physica E (Amsterdam) **1**, 71 (1997).

[51] For a noninteracting system this finite-size correction can be exactly calculated. We find the value $1/(2N-1)$, where N is the particle number; see the inset in Fig. 15.